Supplementary Information

Anticancer Activity of Pt-Selenolate Metallacycles

M. K. Pal[a], A. G. Majumdar[b], K. V. Vivekananda[a], A. P. Wadawale[a], M. Subramanian[b], N. Bhuvanesh[c] and S. Dey[a,d,*]

[a] Chemistry Division, Bhabha Atomic Research Centre, Mumbai 400 085, India

[b] Bio-Organic Division, Bhabha Atomic Research Centre, Mumbai 400 085, India

[c] Department of Chemistry, Texas A&M University, PO Box 30012, College Station, Texas 77842-3012, USA

[d] Homi Bhabha National Institute, Training School Complex, Mumbai-400094, India

** E-mail: dsandip@barc.gov.in (S. Dey); Tel: +91-22-2559-2589*

Table of Contents

Materials and methods

All experiments were carried out under a nitrogen atmosphere by using standard Schlenk technique. Solvents used in the reactions were degassed with nitrogen and distilled using standard procedures. The 4,4′-dipyridyldisulfide (4,4́-py_2S_2) was used as purchased from commercial sources without further purification. The ligand 4,4′-dipyridyldiselenide (4,4́-py_2Se_2[1], the precursor complexes $[Pt(PEt_3)_2(OTf)_2]$, $[Pt(dppe)(OTf)_2]$ and $[Pt(dppf)(OTf)_2]$ [2,3] and the selenolate complexes $[PdCl(PPh_3)_2(4\text{-}Sepy)]$ (**3**), $[PtCl(PEt_3)_2(4\text{-}Sepy)]$ (**4**), $[Pd(dppe)(4\text{-}Sepy)]_n(OTf)_n$ (**5**), $[Pd(dppf)(4\text{-}Sepy)]_n(OTf)_n$ (**8**) and dithiolate complex $[Pt_2(PEt_3)_4(SC_{12}H_8S)]_2(OTf)_4$ (**11**) were prepared by literature methods.[4,5] Melting points were determined in capillary tubes and are uncorrected. Elemental analyses were carried out on a Thermo Fischer Flash EA1112 CHNS analyzer. UV-vis absorption spectra were recorded in dichloromethane using JASCO V-630 spectrophotometer. ^{1}H NMR spectra were recorded on a Bruker and Varian NMR spectrometers operating at 300, 400 and 500 MHz, chemical shifts are relative to internal dichloromethane-d_2 and chloroform-d_1 peak (δ 5.30 and δ 7.26). The chemical shifts (δ) were reported in parts per million (ppm). The coupling constants (*J*) are quoted in Hertz (Hz). Proton splitting patterns are described as s (singlet), d (doublet), t (triplet), and m (multiplet). For $^{31}P\{^1H\}$ NMR spectra were recorded on NMR spectrometer operating at 121.46 and 243.17 MHz, $^{19}F\{^1H\}$, $^{77}Se\{^1H\}$ and $^{195}Pt\{^1H\}$ NMR spectra were recorded on a Bruker NMR spectrometer operating at 282.38, 57.2 and 64.5 MHz respectively. Mass spectra were recorded on a maXis Impact (Bruker) mass spectrometer.

Synthesis of Complexes

[Pt(dppf)(4-Spy)$_2$] (1)

To a methanolic solution (10 ml) of Na(4-Spy) (freshly prepared from 4,4′-py$_2$S$_2$ (19.4 mg, 0.088 mmol) and $NaBH_4$ (8.0 mg, 0.211 mmol)), a dichloromethane solution (10 ml) of [Pt(dppf)Cl_2] (72.2 mg, 0.088 mmol) was added and stirred for 3 h. Solvents were removed using vacuuo to get yellow solid, which was washed with hexane and diethyl ether. The residue was recrystallized from dichloromethane-hexane mixture to afford yellow crystals of the title compound (72.3 mg, 85%), mp > 200 °C. Anal. Calcd for $C_{44}H_{36}N_2P_2S_2PtFe$: C, 54.49; H, 3.74; N, 2.89; Found C, 54.81; H, 3.94; N, 2.61%. UV/vis (dichloromethane): λ_{max} (ε in M^{-1} cm^{-1}) 294 (sh, 7257) nm. ^{1}H NMR (300 MHz, $CDCl_3$) δ: 4.20 (s, 4 H, H$_\beta$-ferr), 4.37 (s, 4 H, H$_\alpha$-ferr), 7.04 (d, $^3J_{H,H}$ = 5.1 Hz, 4H, H$_\beta$-Py), 7.32 (t, $^3J_{H,H}$ = 6.9 Hz, 8H, *m*-H of Ph), 7.41 (d, $^3J_{H,H}$ = 7.2 Hz, 4H, *p*-H of Ph), 7.76 (t, $^3J_{H,H}$ = 8.1 Hz, 8H, *o*-H of Ph), 7.85 (d, $^3J_{H,H}$ = 5.1 Hz, 4H, H$_\alpha$-Py). ^{31}P{^{1}H} NMR (121.5 MHz, $CDCl_3$) δ: 17.6 (s, $^1J_{P\text{-}Pt}$ = 3034 Hz) ppm. ^{195}P{^{1}H} NMR (64.5 MHz, $CDCl_3$) δ: -4685 (t, $^1J_{P\text{-}Pt}$ = 3033 Hz) ppm.

[Pt(dppf)(4-Sepy)$_2$] (2)

Prepared in a similar manner to that for **1**, using 4,4′-py$_2$Se$_2$ (34.0 mg, 0.108 mmol), $NaBH_4$ (9.0 mg, 0.238 mmol) and [Pt(dppf)Cl_2] (88.8 mg, 0.108 mmol) and recrystallized from dichloromethane-hexane mixture to afford orange crystals of the title compound (89.4 mg, 78%), mp > 200 °C. Anal. Calcd for $C_{44}H_{36}N_2P_2Se_2PtFe$: C, 49.69; H, 3.41; N, 2.63; Found C, 49.44; H, 3.58; N, 2.26%. UV/vis (dichloromethane): λ_{max} (ε in M^{-1} cm^{-1}) 294 (sh, 4894) nm. ^{1}H NMR (600 MHz, $CDCl_3$) δ: 4.19 (s, 4H, H$_\beta$-ferr), 4.34 (s, 4H, H$_\alpha$-ferr), 7.18 (d, $^3J_{H,H}$ = 5.4 Hz, 4H, H$_\beta$-Py), 7.35 (t, $^3J_{H,H}$ = 7.5 Hz, 8H, *m*-H of Ph), 7.44 (t, $^3J_{H,H}$ = 7.5 Hz, 4H, *p*-H of Ph), 7.81 (t, $^3J_{H,H}$ = 9.0 Hz, 8H, *o*-H of Ph), 7.85 (d, $^3J_{H,H}$ = 5.4 Hz, 4H, H$_\alpha$-Py). ^{31}P{^{1}H} NMR (243 MHz, $CDCl_3$) δ: 12.2 ($^1J_{P\text{-}Pt}$ = 3083 Hz, $^1J_{P\text{-}Se}$ = 51 Hz) ppm.

X-ray Crystallography

A Rigaku-Oxford make XtaLAB Synergy, Dualflex X-ray diffractometer was employed for crystal screening, unit cell determination, and data collection. The goniometer was controlled using the APEX3 software suite.[6] The X-ray radiation employed was generated from a Mo X-ray tube Kα (λ = 0.71073 Å). Integrated intensity information for each reflection was obtained by reduction of the data frames with the program APEX3.[6] The integration method employed a three-dimensional profiling algorithm and all data were corrected for Lorentz and polarization factors, as well as for crystal decay effects. Finally, the data was merged and scaled to produce a suitable data set. The absorption correction program SADABS[7] was employed to correct the data for absorption effects. Systematic reflection conditions and statistical tests of the data suggested the space group *Cc*. A solution was obtained readily using XT/XS in APEX3.[6,8] Hydrogen atoms were placed in idealized positions and were set riding on the respective parent atoms. All non-hydrogen atoms were refined with anisotropic thermal parameters. The structure was refined (weighted least squares refinement on F^2) to convergence.[8,9] Olex2 was employed for the final data presentation and structure plots.[9]

#Calculations for masked entities

Compd. **1** (218066)

A solvent mask was calculated using PLATON SQUEEZE and 115 electrons were found in a volume of 310 Å3 in 1 void per unit cell. This is consistent with the presence of 1 ((CHCl$_3$)] accounting for 58 electrons per Formula Unit which account for 116 electrons per unit cell

Moiety formula: C_{44} H_{36} Fe N_2 P_2 Pt S_2, C H Cl_3

Molecular formula: $C_{45}H_{37}Cl_3FeN_2P_2PtS_2$

Compd. **7T** (2180268)

A solvent mask was calculated and 1316 electrons were found in a volume of 5155 Å3 in 1 void per unit cell. This is consistent with the presence of 2 [CF_3SO_3H] accounting for 148 and 3 ($CHCl_3$] accounting for 174 electrons per Formula Unit which account for 1288 electrons per unit cell

Moiety formula: C_{156} H_{128} Fe_4 N_4 P_8 Pt_4 S_4, 4(C F_3 O_3 S). [2(C F_3 O_3 S H), 3(C H Cl_3)]

Molecular formula: C_{165} H_{133} Cl_9 F_{18} Fe_4 N_4 O_{18} P_8 Pt_4 S_{10}

Compd. **9T** (2180270**)**

A solvent mask was calculated and 837 electrons were found in a volume of 3278 Å3 in 1 void per unit cell. This is consistent with the presence of 2[CF_3SO_3H] accounting for 148 and 5(CHCl3] accounting for 58 per Formula Unit which account for 824 electrons per unit cell

Moiety formula: C_{156} H_{128} Fe_4 N_4 P_8 Pt_4 Se_4, 4(C F_3 O_3 S), 2(C F_3 O_3 S H), 5($CHCl_3$)

Molecular formula: C_{167} H_{135} Cl_{15} F_{18} Fe_4 N_4 O_{18} P_8 Pt_4 S_6 Se_4

References

1. B. Boduszek and R. Gancarz, *J. Prakt. Chem.*, 1996, **338**, 186−189.
2. P. A. Mane, S. Dey, A. K. Pathak, M. Kumar, N. Bhuvanesh, *Inorg. Chem.,* 2019, **58**, 2965−2978.
3. P. J. Stang, B. Olenyuk, J. Fan and A. M. Arif, *Organometallics*, 1996, **15**, 904−908.
4. K. V. Vivekananda, S. Dey, A. Wadawale, N. Bhuvanesh, V. K. Jain, *Dalton Trans*., 2013, **42**, 14158.
5. P. A. Mane, A. K. Pathak, N. Bhuvanesh and S. Dey, *Inorg. Chem. Front.*, 2021, **8**, 3815−3829.
6. APEX3 “Program for Data Collection on Area Detectors” BRUKER AXS Inc., 5465 East Cheryl Parkway, Madison, WI 53711−5373 USA.

7. G. M. Sheldrick, SADABS, “Program for Absorption Correction of Area Detector Frames”, BRUKER AXS Inc., 5465 East Cheryl Parkway, Madison, WI 53711−5373 USA.
8. (a) G. M. Sheldrick, *Acta Cryst.*, 2008, **A64**, 112−122. (b) G. M. Sheldrick, *Acta Cryst.*, 2015, **A71**, 3−8. (c) G. M. Sheldrick, *Acta Cryst.*, 2015, **C71**, 3−8. XT, XS, BRUKER AXS Inc., 5465 East Cheryl Parkway, Madison, WI 53711−5373 USA.
9. O. V. Dolomanov, L. J. Bourhis, R. J. Gildea, J. A. K. Howard and H. Puschmann, “OLEX2: A Complete Structure Solution, Refinement and Analysis Program”, *J. Appl. Cryst.,* 2009, **42**, 339−341.

CT-DNA Interaction Studies

The stock solution of CT-DNA was prepared by dissolving requisite amount of DNA in Tris-HCl buffer solution (10 mM; pH = 7.5). The ratio of UV-Vis absorbance at 260 nm and 280 nm of the solution (calcd. 1.85) indicates that CT-DNA sample doesn’t have any protein contamination. The concentration of the DNA stock solution was measured by considering the molar extinction coefficient of the CT-DNA at 260 nm to be 6600 M^{-1} cm^{-1}. The stock solution of the complex was prepared in DMSO-buffer mixture (v/v = 1:1000). All the data were recorded at room temperature. The absorption study was performed by maintaining the concentration of the complex constant and varying DNA concentration. The absorption spectra were recorded for $[Pt(dppf)(4\text{-}Spy)]_n(OTf)_n$ (**7**) (22 μM) followed by gradual addition of the CT-DNA solution (for range of 0–4.32 μM). The spectra were recorded after equilibration for 5 min, allowing the complexes to bind to the CT-DNA.

Biological evaluation

Cell viability assay. IC_{50} values of the different compounds against MCF-7 cells were determined using the MTT assay. Briefly, 7.5×10^3 cells were seeded in 96 well plates; 16 h

post seeding, cells were treated with different concentrations of the compounds (in triplicates) and incubated for 48 h. For determining cellular viability post treatment, the culture medium was replaced with medium containing 0.5 mg/mL of 3-(4,5-dimethylthiazol-2-yl)-2,5-diphenyl tetrazolium bromide (MTT) reagent. Cells were incubated for 4 h, followed by dissolution of the formazan crystals in DMSO. Absorbance was recorded at 570 nm in a microplate reader (Omega series, BMG Labtech). Percentage viability at each concentration of compound was calculated on the basis of the absorbance of the respective untreated sample.

Clonogenic assay. Colony formation (clonogenic) assay was used to evaluate the effect of the compounds on cellular viability of MCF-7 cells. Briefly, 500 cells were seeded in a 6 well plates, followed by 16 h incubation to facilitate cellular attachment. Post attachment, cells were treated with different concentrations of the compounds, and incubated for 12 days. Colonies were then fixed with 3.5% paraformaldehyde, followed by staining with a 0.5% crystal violet solution. Post staining, colonies were counted under a light microscope. Colonies containing more than 30 cells were considered for calculations. Percentage survival was calculated based on normalization with the corresponding untreated samples.

Cell cycle analysis. The effect of different compounds on the cell cycle distribution of MCF-7 cells was determined using flow cytometry. Briefly, 2×10^5 cells were seeded in 6 well plates; 16 h post seeding, cells were treated with different concentrations of the compounds and incubated for 24 h, followed by flow cytometric analysis. Cells were collected by trypsinization, and washed once with phosphate buffered saline (PBS). Cells were then resuspended in propidium iodide staining buffer (1% sodium citrate and 0.1% Triton X-100, supplemented with 50 µg/mL propidium iodide and 25 µg/mL RNase A). Cells were incubated in staining buffer for 30 minutes, followed by analysis on a CyFlow Space (Sysmex-Partec) flow cytometer.

Sub-G1 assay. Induction of apoptosis by different compounds was evaluated using Sub-G1 analysis. Briefly, 2×10^5 cells were seeded in 6 well plates. Cells were allowed to attach for 16 hours, followed by treatment with different concentrations of the compounds. Cells were incubated for 48 h, followed by sample processing using the process described above for cell cycle analysis.

Annexin V/Propidium Iodide Dual Staining. Induction of early and late apoptotic populations and necrosis was assayed employing Annexin V/Propidium dual staining assay. Briefly, 1.5 x 10^5 MCF-7 cells were seeded per well in 6-well plates, followed by incubation for 16 hours. Cells were then treated with IC_{50} concentrations of relevant compounds for 24 hours, followed by Annexin V/PI dual staining using Annexin V/PI apoptosis detection kit according to manufacturer's protocol. Staining was followed by analysis on a CyFlow Space (Sysmex-Partec) flow cytometer. Flow cytometric data was analyzed using FlowJo software.

Immunofluorescence staining. Induction of DNA damage was assessed using visualization of γ-H2AX foci by means of immunofluorescence staining and confocal microscopy. Briefly, 2×10^5 cells were seeded in 6 well plates on glass coverslips, followed by incubation for 16 hours to facilitate cellular attachment. Post incubation, cells were treated with 2.5 μM of each compound for 24 hours, followed by immunofluorescence staining. Cells were fixed in a 3.5 % paraformaldehyde solution, followed by permeabilization using PBS supplemented with 0.1 % Triton X-100. Permeabilized cells were blocked for 2 h using a 5 % BSA prepared in PBS supplement with 0.1% Tween 20. Cells were then treated with primary antibody (1:1000 dilution in PBS containing 0.1% Tween 20 and 2.5 % BSA) for 16 h at 4 °C. Samples were then treated with AlexaFluor 488 tagged secondary antibody (1:2500 dilution in PBS containing 0.1% Tween 20 and 2.5 % BSA) for 3 hours. Cells were washed thrice with PBS containing 0.1% Tween 20, followed by drying and mounting on glass slides using a solution of 10 μg/mL Hoechst 33258 in 80 % glycerol. Samples were then visualized under a Zeiss

LSM 780 confocal microscope. For quantification of γ-H2AX foci, a minimum of 10 random fields were captured and number of cells containing γ-H2AX foci were calculated as a percentage of total number of cells in each field.

Cellular uptake

Cellular uptake of test compounds was estimated using GFAAS-based estimation of platinum concentration in cells treated with the test compounds. Briefly, 5 x 10^6 cells were seeded in 150 mm dishes, and cells were allowed to attach for 16 hours. Cells were then treated with 10 µM concentration of each compound for 8 hours. Cells were then harvested, and 10 % of cells were removed for protein estimation. The remaining cell pellet was extracted with 500 µL of concentrated nitric acid for 1 hour on ice. The extract was then centrifuged at 4000 rpm for 10 minutes at 4 ℃ to remove cellular debris. The supernatant was collected and subjected to GFAAS. Protein estimation was performed using the Bradford assay. The total protein in the entire cell pellet was back calculated, and the platinum concentration obtained through GFAAS was normalized with the total protein yield of each sample.

Table S1 Crystallographic and structure refinement data for [Pt(dppf)(4-Spy)$_2$]·$CHCl_3$ (**1**·$CHCl_3$) and [Pt(dppf)(4-Sepy)$_2$]·$2CH_2Cl_2$ (**2**·$2CH_2Cl_2$)

Compounds	**1**·$CHCl_3$	**2**·$2CH_2Cl_2$
Chemical Formula	$C_{45}H_{37}Cl_3FeN_2P_2PtS_2$	$C_{46}H_{40}Cl_4FeN_2P_2PtSe_2$
Formula weight	1089.11	1233.40
Crystal Size (mm^3)	0.30 x 0.30 x 0.15	0.30 x 0.30 x 0.02
T/K	298(2)	100(2)
λ/Å	MoKα (λ = 0.71073 Å)	MoKα (λ = 0.71073 Å)
Crystal system	Triclinic	Monoclinic
Space group	$P\bar{1}$	P 21/c
a/Å	9.91430(10)	23.7129(7)
b/Å	12.5170(2)	10.2790(2)
c/Å	18.0875(5)	19.4397(5)
α/º	83.9050(10)	90
β/º	76.9550(10)	112.458(3)
γ/º	80.5420(10)	90
V/$Å^3$	2151.38(6)	4379.0(2)
ρ_{calc}/g cm^{-3}	1.681	1.871
Z	2	4
μ/mm^{-1}	3.978	5.539
Reflection collected/ unique	41553/ 10798	49730/ 11291
Data/restraints/parameters	10798 / 48/ 469	11291/ 67/ 542
Final R_1, wR_2 indices	R1 = 0.0258, wR2 = 0.0557	R1 = 0.0289, wR2 = 0.0630
R_1, wR_2 (all data)	R1 = 0.0334, wR2 = 0.0572	R1 = 0.0404, wR2 = 0.0660
Largest diff. peak & hole [$eÅ^{-3}$]	1.109 and -0.788	1.326 and -1.180

Table S2 Crystallographic and structure refinement data for $[Pt(dppf)(Sepy)]_2(O_3SCF_3)_2 \cdot CH_2Cl_2$ (**9D**$\cdot CH_2Cl_2$) and $[Pt(dppe)(4\text{-}Sepy)]_2(BPh_4)_2 \cdot 4CH_2Cl_2$ (**12D**$\cdot 4CH_2Cl_2$).

Compounds	**9D**$\cdot CH_2Cl_2$	**12D**$\cdot 4CH_2Cl_2$
Chemical Formula	$C_{81}H_{66}Cl_2F_6Fe_2N_2O_6P_4Pt_2S_2Se_2$	$C_{114}H_{104}B_2Cl_8N_2P_4Pt_2Se_2$
Formula weight	2196.05	2479.19
Crystal Size (mm^3)	0.50 x 0.50 x 0.10	0.16×0.14×0.06
T/K	298(2)	150.15
λ/Å	CuKα (λ = 1.54184Å)	MoKα (λ = 0.71073 Å)
Crystal system	Monoclinic	triclinic
Space group	P 21/c	$P\,\bar{1}$
a/Å	12.8799(2)	11.5598(19)
b/Å	16.5012(3)	15.143(2)
c/Å	38.1414(5)	15.801(3)
α/°	90	86.121(2)
β/°	98.2750(10)	72.408(2)
γ/°	90	84.689(2)
V/Å^3	8021.9(2)	2622.9(7)
ρ_{calc}/g cm^{-3}	1.818	1.570
Z	4	1
μ/mm^{-1}	12.676	3.672
Reflection collected/ unique	129978/ 15811	48295/ 11872
Data/restraints/parameters	15811/ 392/ 1084	11872/7/602
Final R_1, wR_2 indices	R1 = 0.0412, wR2 = 0.0932	R_1 = 0.0366, wR_2 = 0.0753
R_1, wR_2 (all data)	R1 = 0.0601, wR2 = 0.1019	R_1 = 0.0503, wR_2 = 0.0826
Largest diff. peak & hole [eÅ^{-3}]	0.92 and -1.31	2.091and -2.668

Table S3 Crystallographic and structure refinement data for $[Pt(dppf)(Spy)]_4(O_3SCF_3)_4$ (**7T**·$3CHCl_3$·$2CF_3SO_3H$) and $[Pt(dppf)(Sepy)]_4(O_3SCF_3)_4$·$5CHCl_3$·$2CF_3SO_3H$ (**9T**·$5CHCl_3$·$2CF_3SO_3H$).

Compounds	**7T**·$3CHCl_3$·$2CF_3SO_3H$	**9T**·$5CHCl_3$·$2CF_3SO_3H$
Chemical Formula	$C_{165}H_{133}Cl_9F_{18}Fe_4N_4O_{18}P_8Pt_4S_{10}$	$C_{167}H_{135}Cl_{15}F_{18}Fe_4N_4O_{18}P_8Pt_4S_6Se_4$
Formula weight	4692.92	5119.25
Crystal Size (mm^3)	0.20 x 0.20 x 0.10	0.30 x 0.20 x 0.10
T/K	298(2)	298(2)
λ/Å	CuKα (λ = 1.54184 Å)	MoKα (λ = 0.71073 Å)
Crystal system	Tetragonal	Tetragonal
Space group	*I* 4_1/a	*I* 4_1/a
a/Å	19.9324(4)	20.2575(3)
b/Å	19.9324(4)	20.2575(3)
c/Å	47.0921(19)	47.4559(10)
α/°	90	90
β/°	90	90
γ/°	90	90
V/$Å^3$	18709.7(11)	19474.3(7)
ρ_{calc}/g cm^{-3}	1.666	1.746
Z	4	4
μ/mm^{-1}	11.385	4.310
Reflection collected/ unique	33113/ 9333	45274/ 12125
Data/restraints/parameters	9333/ 61 / 479	12125/ 76/ 527
Final R_1, wR_2 indices	R1 = 0.0520, wR2 = 0.1426	R1 = 0.0328, wR2 = 0.0849
R_1, wR_2 (all data)	R1 = 0.0696, wR2 = 0.1570	R1 = 0.0510, wR2 = 0.0937
Largest diff. peak & hole [$eÅ^{-3}$]	1.584 and -0.995	0.952 and -0.553

Table S4 Calculated and experimental peaks of the fragmented ions of [Pt(dppf)(4-Spy)]$_n$(OTf)$_n$ (**7**).

m/z	Ion	Calculated peak of the most abundant ion	Experimental peak of the most abundant ion
2875.12	($[M_3 – OTf]^+$, 19%)	2876.12	2876.12
4295.36/2 = 2147.68	($[M_5 − 5OTf]^{2+}$, 2%)	2148.68	2148.64
4231.33/2 = 2116.66	($[M_5 – (5OTf + C_5H_4)]^{2+}$, 2%)	2116.65	2116.65
1867.10	($[M_2 – OTf]^+$, 53%)	1868.10	1868.09
3586.25/2 = 1793.13	($[M_4 + H – 3OTf]^{2+}$, 7%)	1794.12	1794.10
1738.97	($[M_3 + 2CH_3CN – (2dppf + Spy + OTf)]^+$, 17%)	1739.96	1739.99
1718.15	($[M_2 – 2OTf]^+$, 15%)	1719.15	1719.14
1641.11	($[M_2 – (2OTf + Ph)]^+$, 46%)	1641.11	1641.12
1630.85	($[M_2 – 5Ph]^+$, 68%)	1630.85	1631.01
1531.10	($[M_2 – (2OTf + Spy + Ph)]^+$, 100%)	1531.10	1531.13
1499.14	($[M_2 + H – (2OTf + Spy)]^+$, 70%)	1499.14	1499.15
2825.02/2 = 1412.51	($[M_4 + 2CH_3CN – (2dppf + S + OTf)]^{2+}$, 21%)	1413.01	1413.02
2726.17/2 = 1363.08	($[M_3 − 2OTf]^{2+}$, 63%)	1363.58	1363.59

Table S5 Calculated and experimental peaks of the fragmented ions of [Pt(dppf)(4-Sepy)]$_n$(OTf)$_n$ (**9**).

m/z	Ion	Calculated peak of the most abundant ion	Experimental peak of the most abundant ion
2665.40/2 = 1332.70	([M_4 + H – (dppf + Sepy + 11Ph)]$^{2+}$, 2%)	1331.71	1331.53
2669.83/2 = 1334.91	([M_4 + H – (2dppf + 3OTf)]$^{2+}$, 2%)	1333.92	1334.08
2894.70/2 = 1447.35	([M_4 + 2CH_3CN – (2dppf + OTf + 2Ph)]$^{2+}$, 4%)	1446.35	1446.16
2900.39/2 = 1450.19	([M_4 + H – (dppf + 10Ph)]$^{2+}$, 9%)	1449.20	1449.14
1625.08	([M_2 + 3CH_3CN – (2OTf + Sepy + 2Ph)]$^{+}$, 23%)	1625.09	1625.15
1666.99	([M_2 + 2CH_3CN + 2H – (2OTf + 3Ph)]$^{+}$, 26%)	1666.00	1666.08
1688.11	([M_2 + CH_3OH – (2OTf + Sepy)]$^{+}$, 100%)	1688.11	1688.08
1736.00	([M_2 – (2OTf + py)]$^{+}$, 75%)	1735.01	1735.11

Table S6 Calculated and experimental peaks of the fragmented ions of $[Pt(PEt_3)_2(4\text{-}Sepy)]_n(OTf)_n$ (**10**).

m/z	Ion	Calculated peak of the most abundant ion	Experimental peak of the most abundant ion
1944.04	$([M_4 – (4OTf + 3PEt_3 + 2Et)]^+$, 2%)	1941.04	1940.94
1866.01	$([M_4 – (4OTf + 3PEt_3 + py + 2Et)]^+$, 2%)	1863.01	1863.01
1713.98	$([M_4 + H – (3OTf + Pt(PEt_3)_2 + Sepy + 7Et)]^+$, 2%)	1711.98	1712.05
1595.07	$([M_4 + 2H – (4OTf + Pt(PEt_3)_2 + Sepy + 6Et)]^+$, 12%)	1593.08	1593.04
1381.17	$([M_2 + 2CH_3CN + H – (OTf + Et)]^+$, 100%)	1381.17	1381.16
1327.15	$([M_2 – OTf]^+$, 33%)	1326.15	1326.14
1311.08	$([M_2 + 2H – (Se + 3Et)]^+$, 74%)	1311.08	1311.13
1231.21	$([M_2 + 2CH_3CN – (2OTf + Et)]^+$, 36%)	1230.21	1230.20
1216.00	$([M_2 + CH_3CN + 2H – (5Et + Sepy)]^+$, 14%)	1216.00	1216.06
1204.19	$([M_2 + 2CH_3CN + 2H – (2OTf + 2Et)]^+$, 35%)	1202.19	1202.19

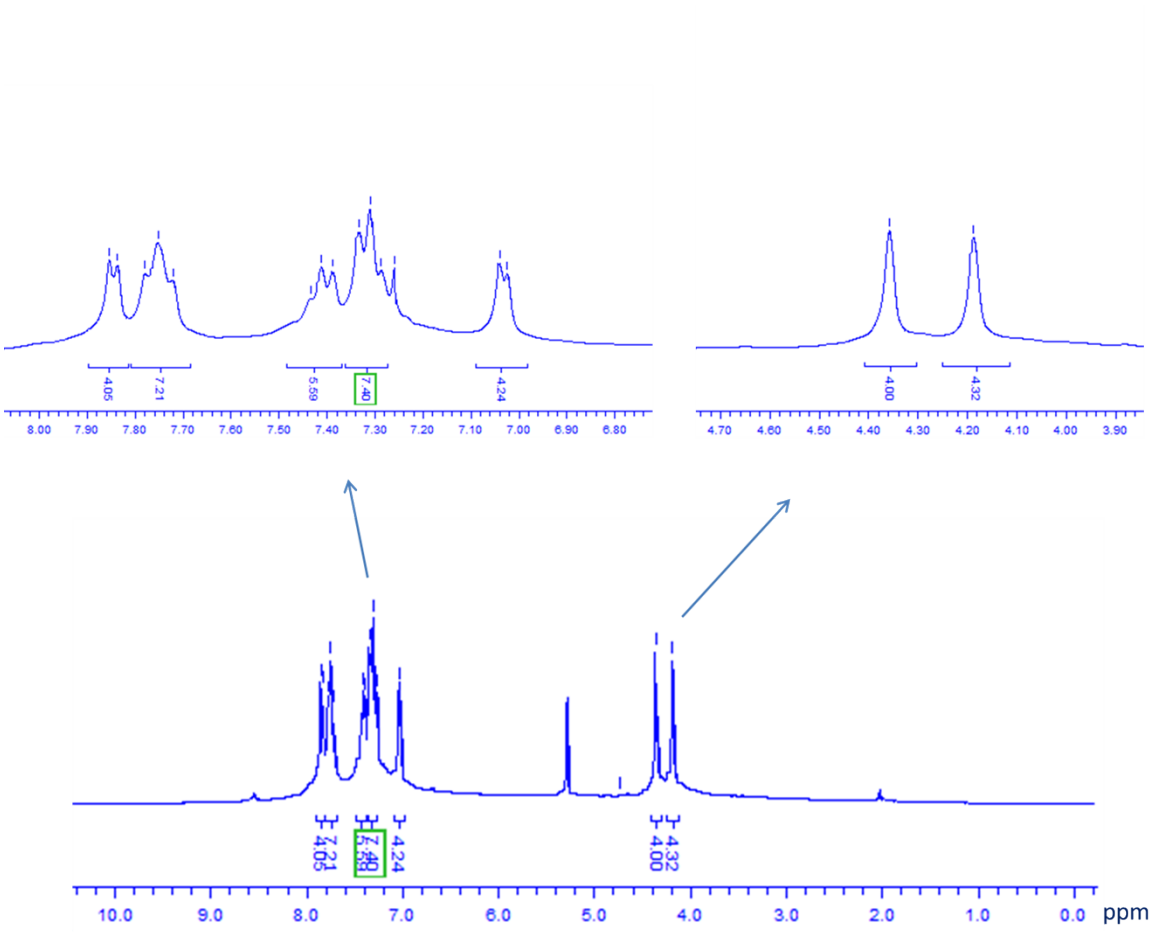

Fig. S1 ^{1}H NMR spectra (300 MHz, $CDCl_3$) of [Pt(dppf)(4-Spy)$_2$] (**1**).

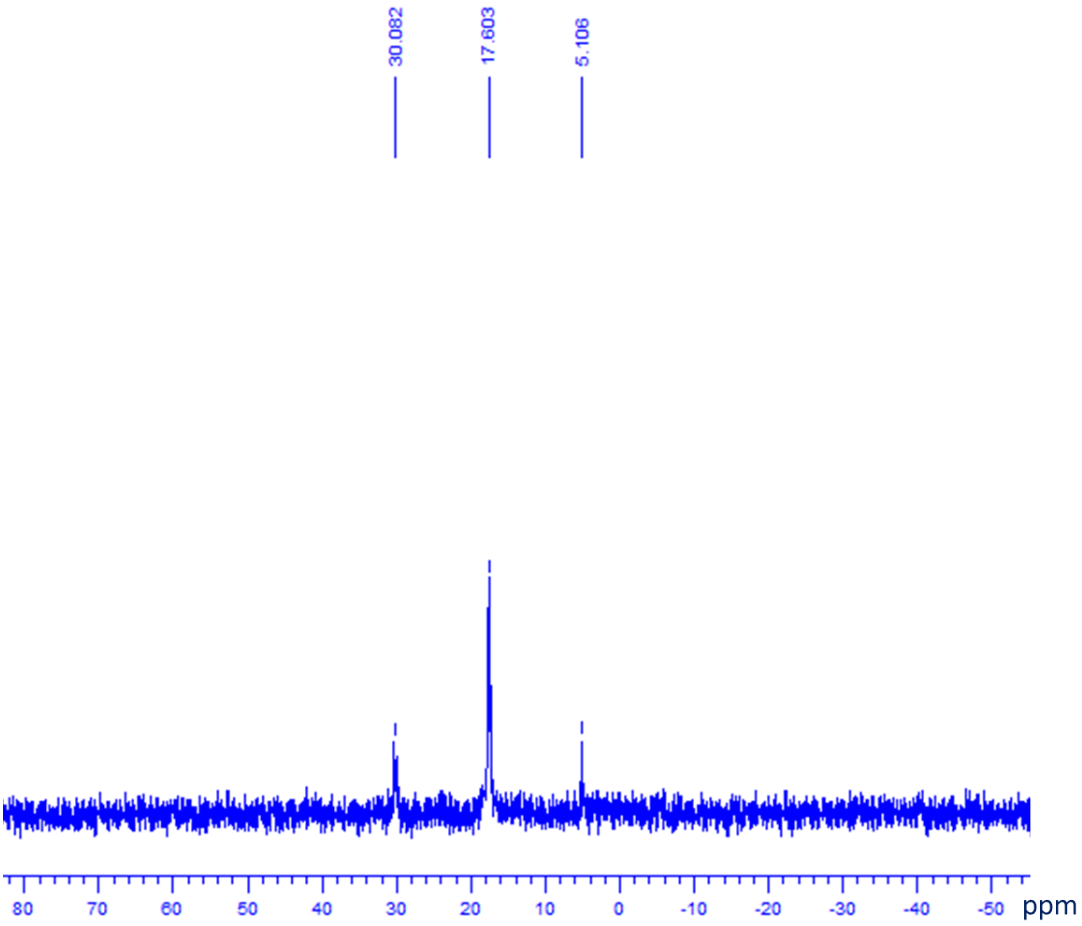

Fig. S2 $^{31}P\{^{1}H\}$ NMR spectra 121.5 MHz, $CDCl_3$) of [Pt(dppf)(4-Spy)$_2$] (**1**).

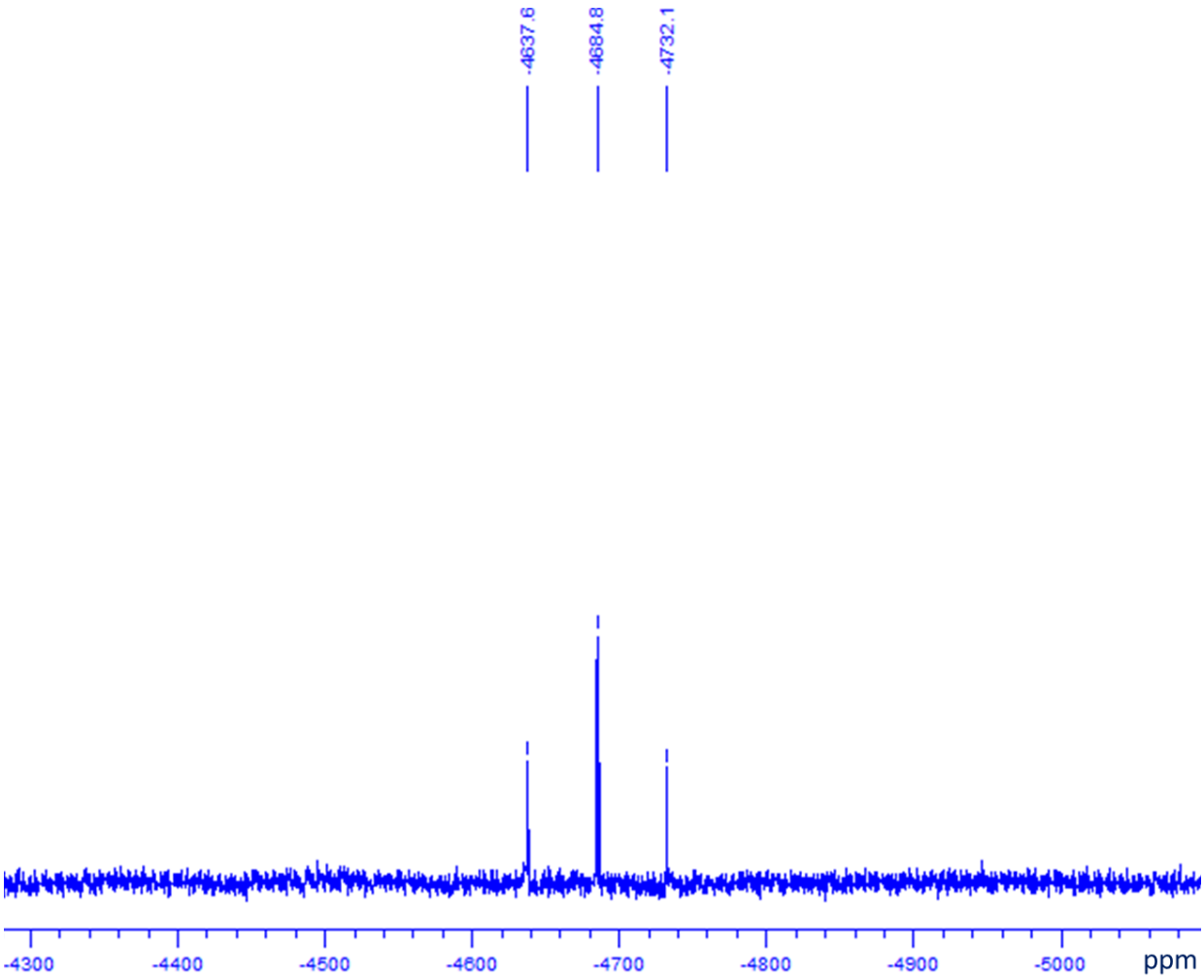

Fig. S3 $^{195}Pt\{^{1}H\}$ NMR spectra 64.5 MHz, $CDCl_3$) of [Pt(dppf)(4-Spy)$_2$] (**1**).

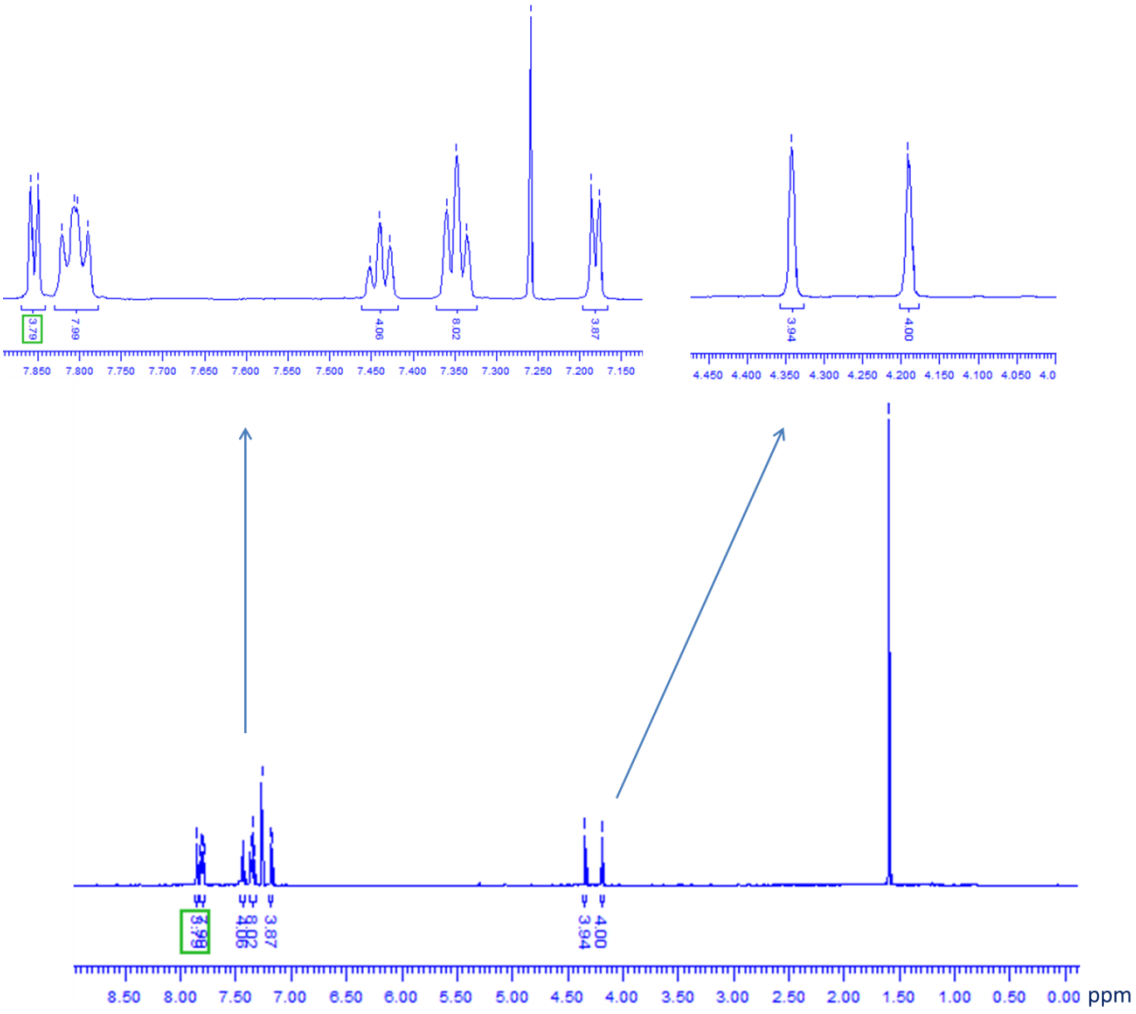

Fig. S4 ^{1}H NMR spectra (600 MHz, $CDCl_3$) of [Pt(dppf)(4-Sepy)$_2$] (**2**).

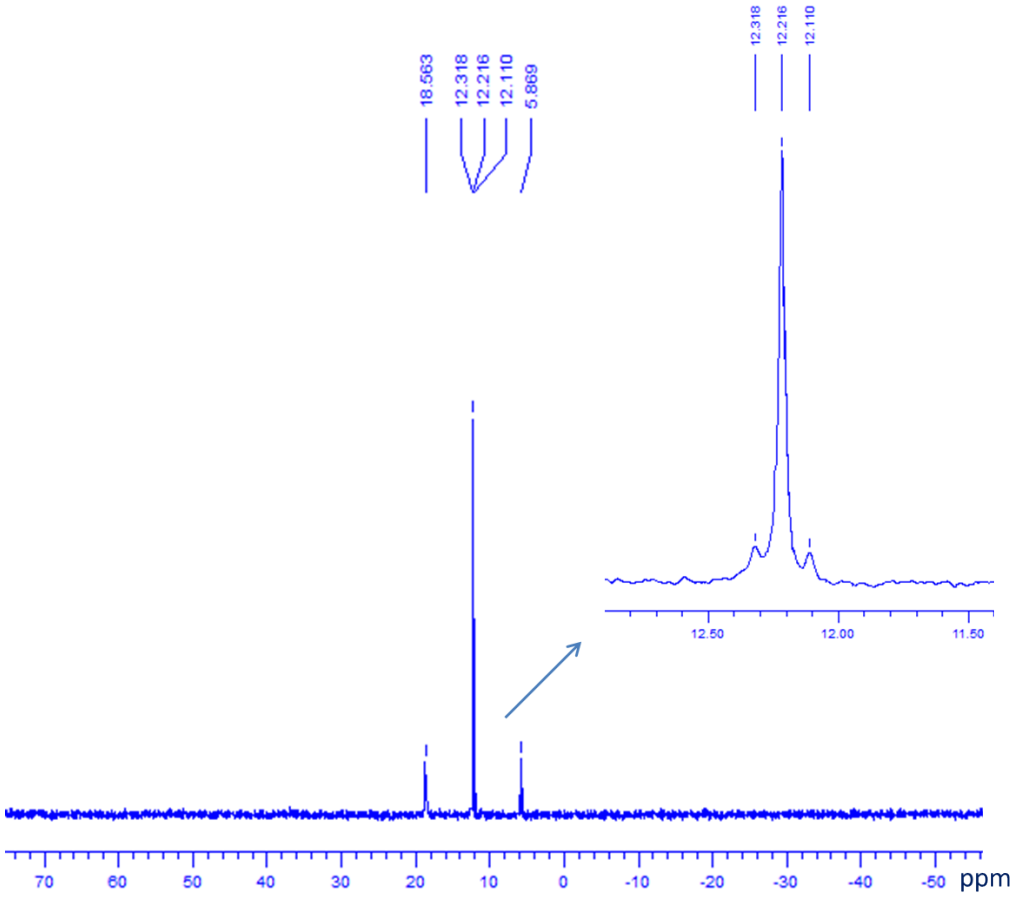

Fig. S5 $^{31}P\{^{1}H\}$ NMR spectra (243 MHz, $CDCl_3$) of [Pt(dppf)(4-Sepy)$_2$] (**2**).

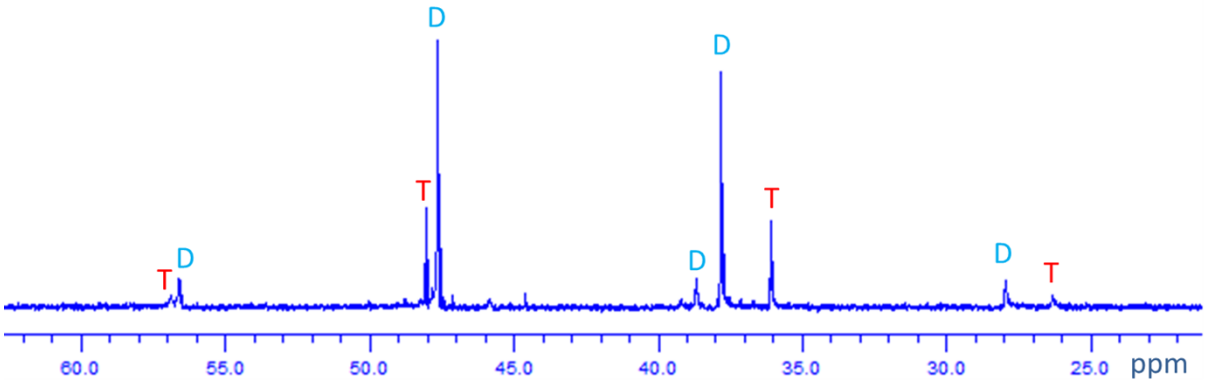

Fig. S6 $^{31}P\{^{1}H\}$ NMR spectra 162 MHz, CD_2Cl_2) of $[Pt(dppe)(4\text{-}Sepy)]_n(OTf)_n$ (**6**).

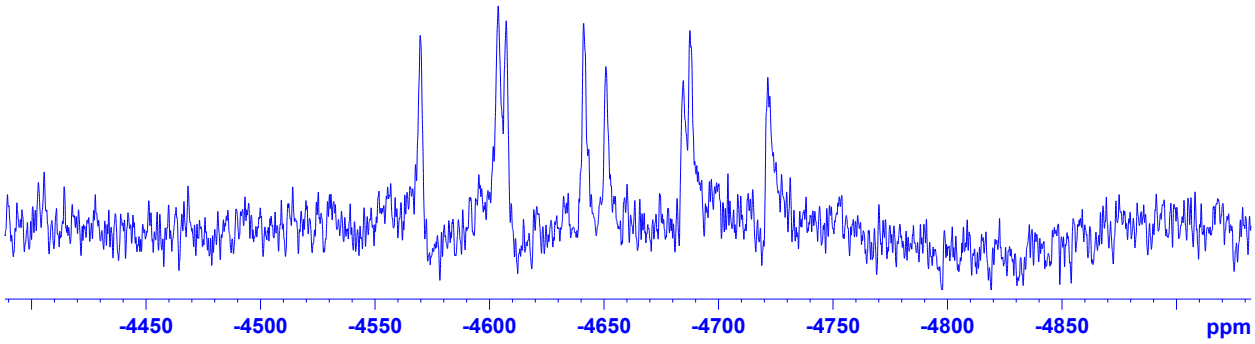

Fig. S7 $^{195}Pt\{^{1}H\}$ NMR (85.6 MHz, CD_2Cl_2) spectra of $[Pt(dppe)(4\text{-}Sepy)]_n(OTf)_n$ (**6**)

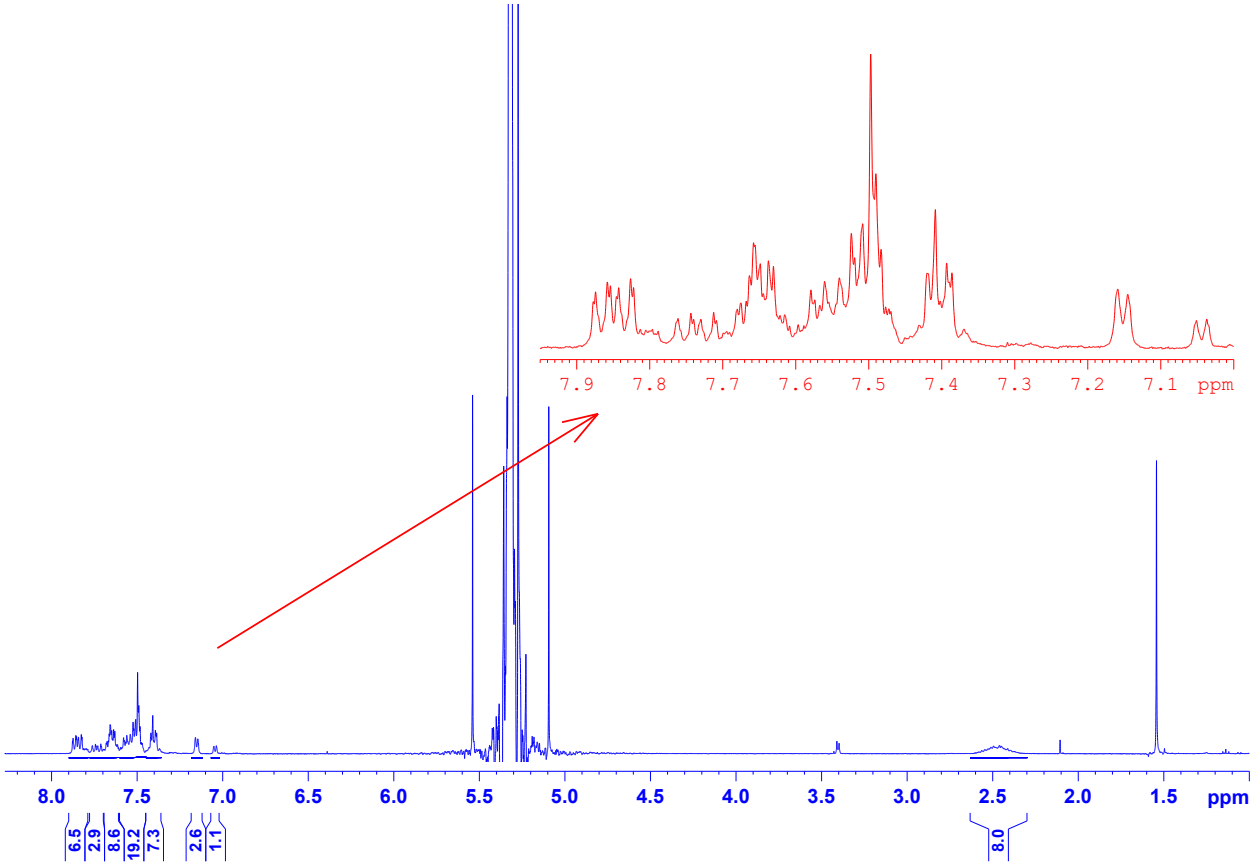

Fig. S8 ^{1}H NMR spectra (400 MHz, CD_2Cl_2) of $[Pt(dppe)(4\text{-}Sepy)]_n(OTf)_n$ (**6**)

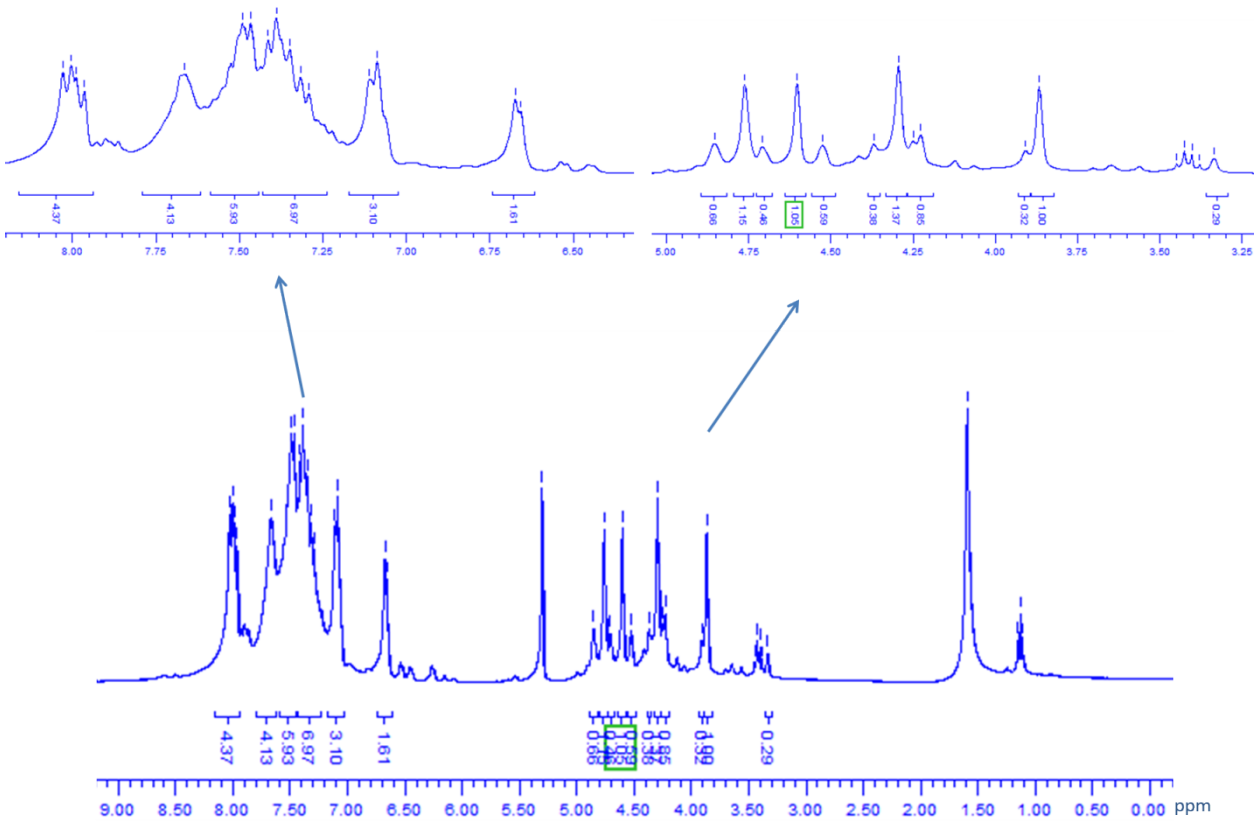

Fig. S9 ^{1}H NMR spectra (300 MHz, CD_2Cl_2) of $[Pt(dppf)(4\text{-}Spy)]_n(OTf)_n$ (**7**) obtained from reaction between **[**$Pt(dppf)(4\text{-}Spy)_2$] (**1)** and $Pt(dppf)(OTf)_2$ in 1:1 stoichiometry.

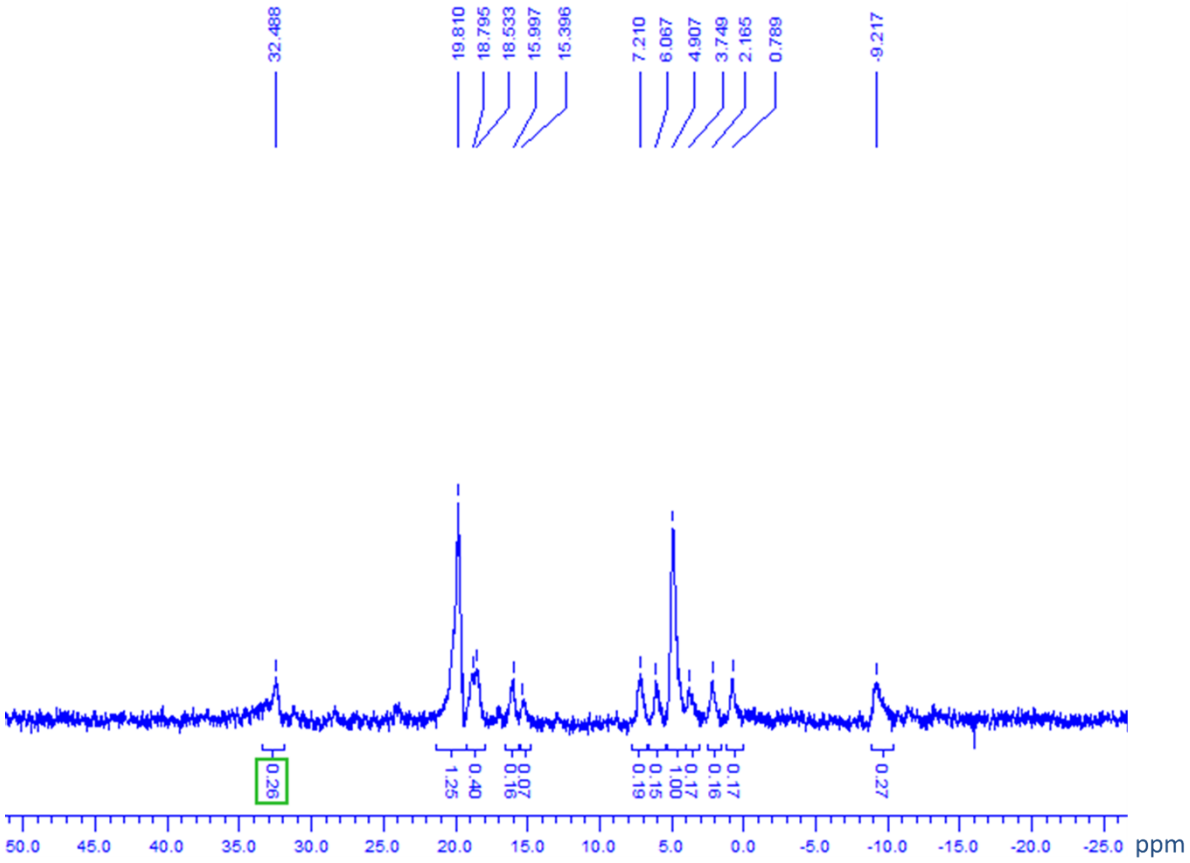

Fig. S10 $^{31}P\{^{1}H\}$ NMR spectra (121.5 MHz, CD_2Cl_2) of $[Pt(dppf)(4\text{-}Spy)]_n(OTf)_n$ (**7**) obtained from reaction between **[**$Pt(dppf)(4\text{-}Spy)_2$] (**1)** and $Pt(dppf)(OTf)_2$ in 1:1 stoichiometry.

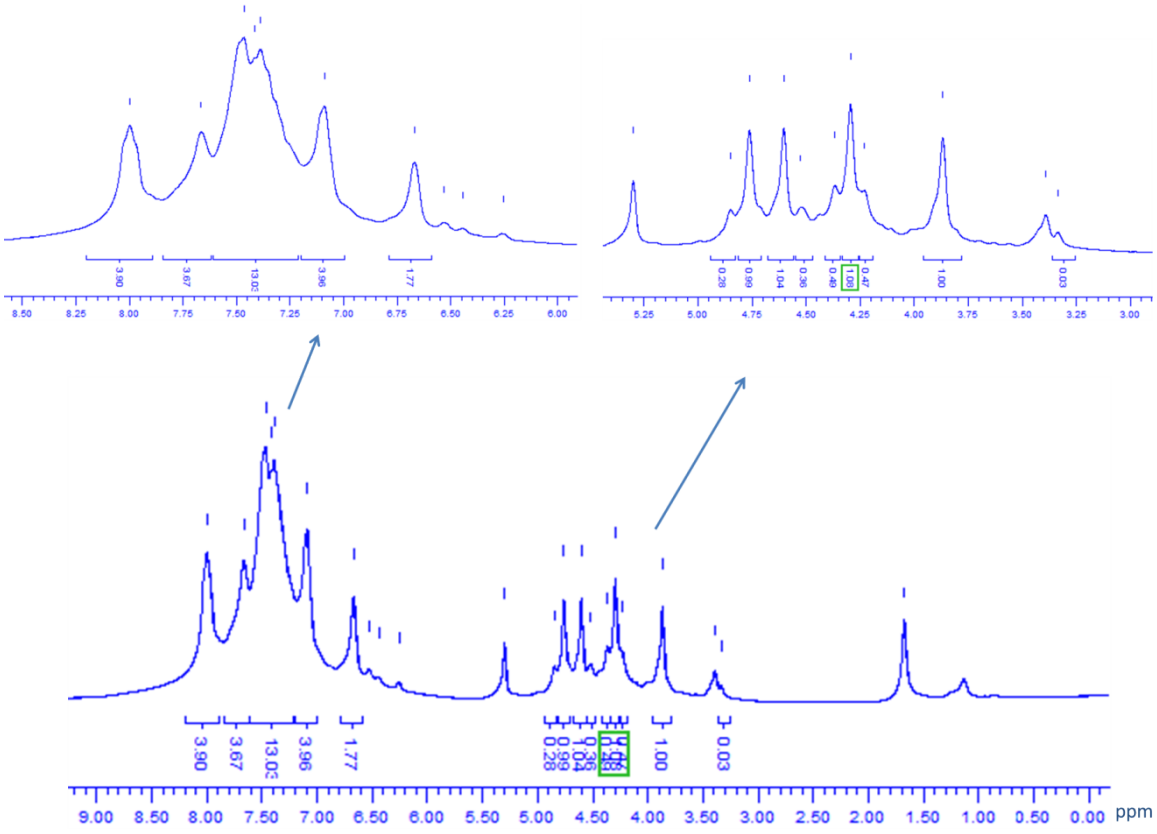

Fig. S11 ^{1}H NMR spectra (300 MHz, CD_2Cl_2) of $[Pt(dppf)(4\text{-Spy})]_n(OTf)_n$ (**7**) obtained from reaction between Na(4-Spy) and $Pt(dppf)(OTf)_2$ in 1:1 stoichiometry.

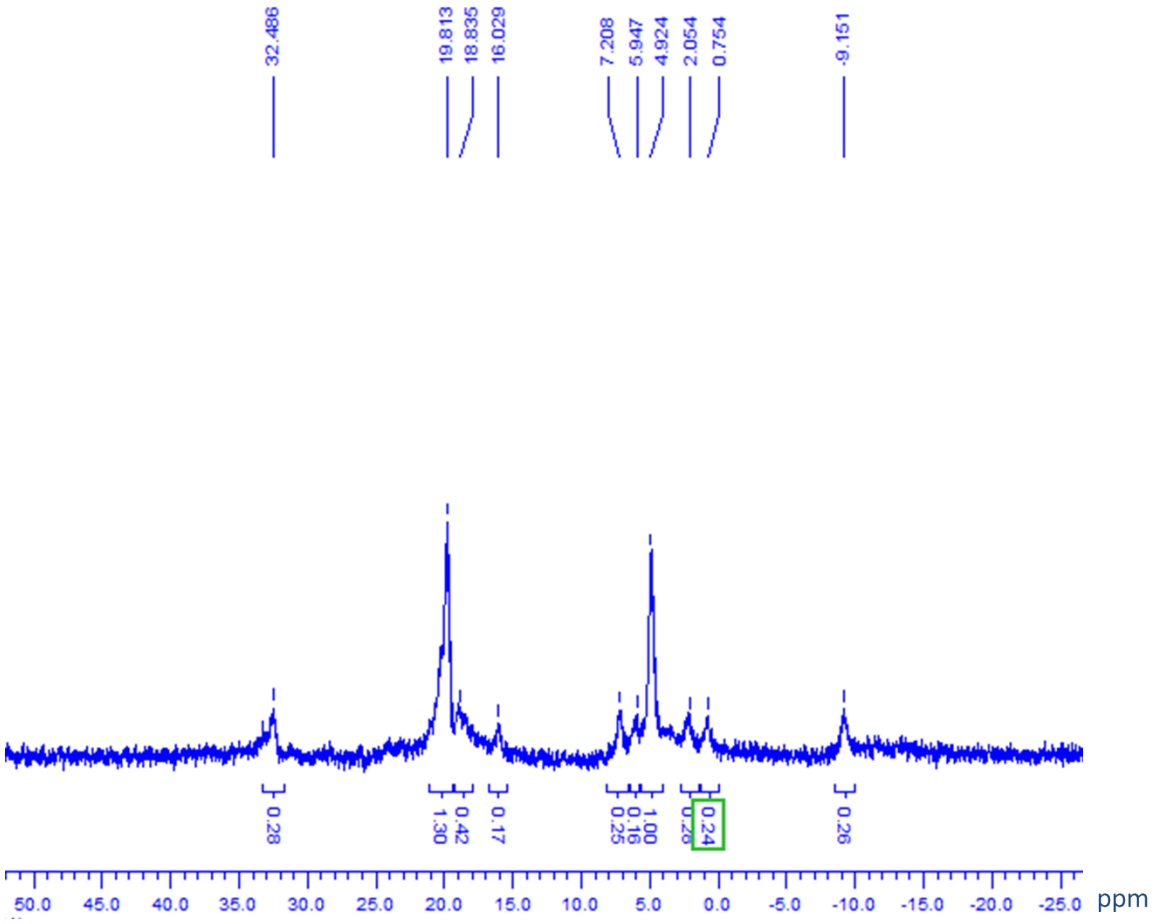

Fig. S12 $^{31}P\{^{1}H\}$ NMR spectra (121.5 MHz, CD_2Cl_2) of $[Pt(dppf)(4\text{-}Spy)]_n(OTf)_n$ (**7**) obtained from reaction between Na(4-Spy) and $Pt(dppf)(OTf)_2$ in 1:1 stoichiometry.

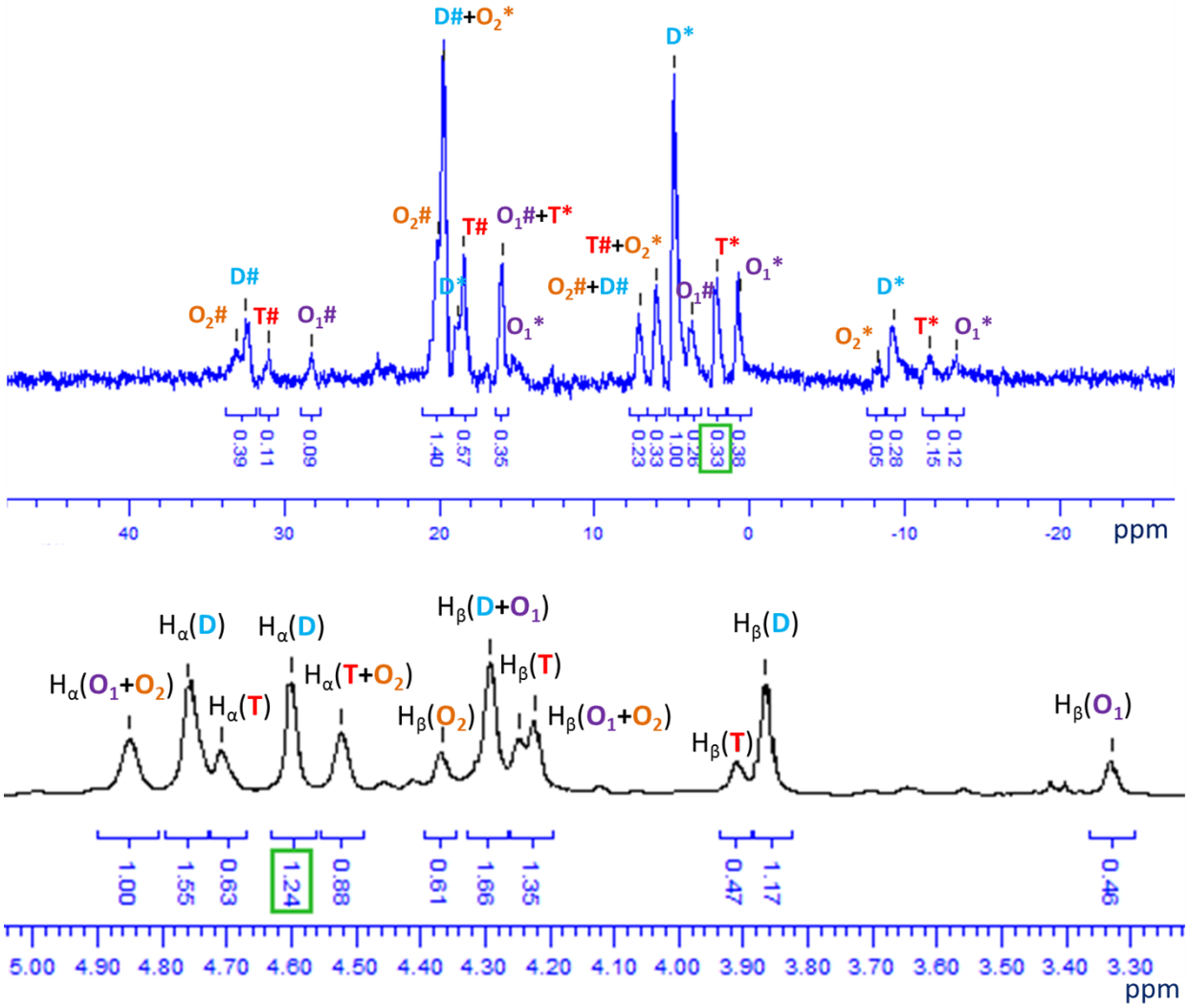

Fig. S13 (A) $^{31}P\{^{1}H\}$ NMR spectrum (121.5 MHz); (**B**) Ferrocenyl region of the ^{1}H NMR spectrum (300 MHz) of $[Pt(dppf)(4\text{-}Spy)]_n(OTf)_n$ (**7**) in CD_2Cl_2 (**D** = dimer **7D**, **T** = tetramer **7T**, $\mathbf{O_1}$ = oligomer 1, $\mathbf{O_2}$ = oligomer 2) obtained from reaction between **[**$Pt(dppf)(4\text{-}Spy)_2$] (**1**) and $Pt(dppf)(OTf)_2$ in 1:1 stoichiometry in NMR tube after 5days.

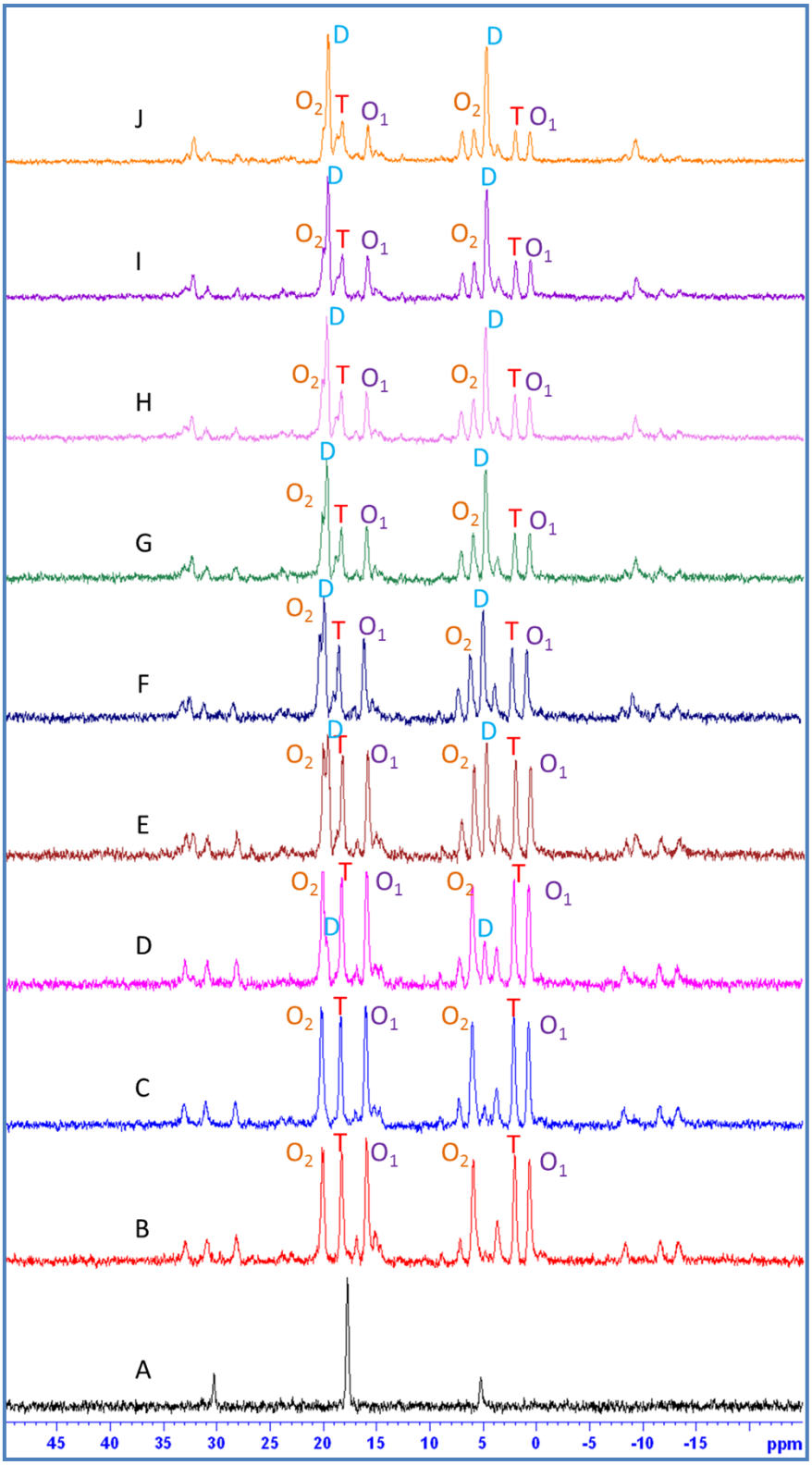

Fig. S14 $^{31}P\{^{1}H\}$ NMR (121.5 MHZ, CD_2Cl_2) spectra of (A) [Ptdppf(4-Spy)$_2$] (**1**), (B) [Ptdppf(4-Spy)$_2$] (**1**) + [Ptdppf(OTf)$_2$] immediately, After (C) 2 h, (D) 6 h, (E) 24 h, (F) 30 h, (G) 48 h, (H) 54 h, (I) 5 days, (J) 6 days.

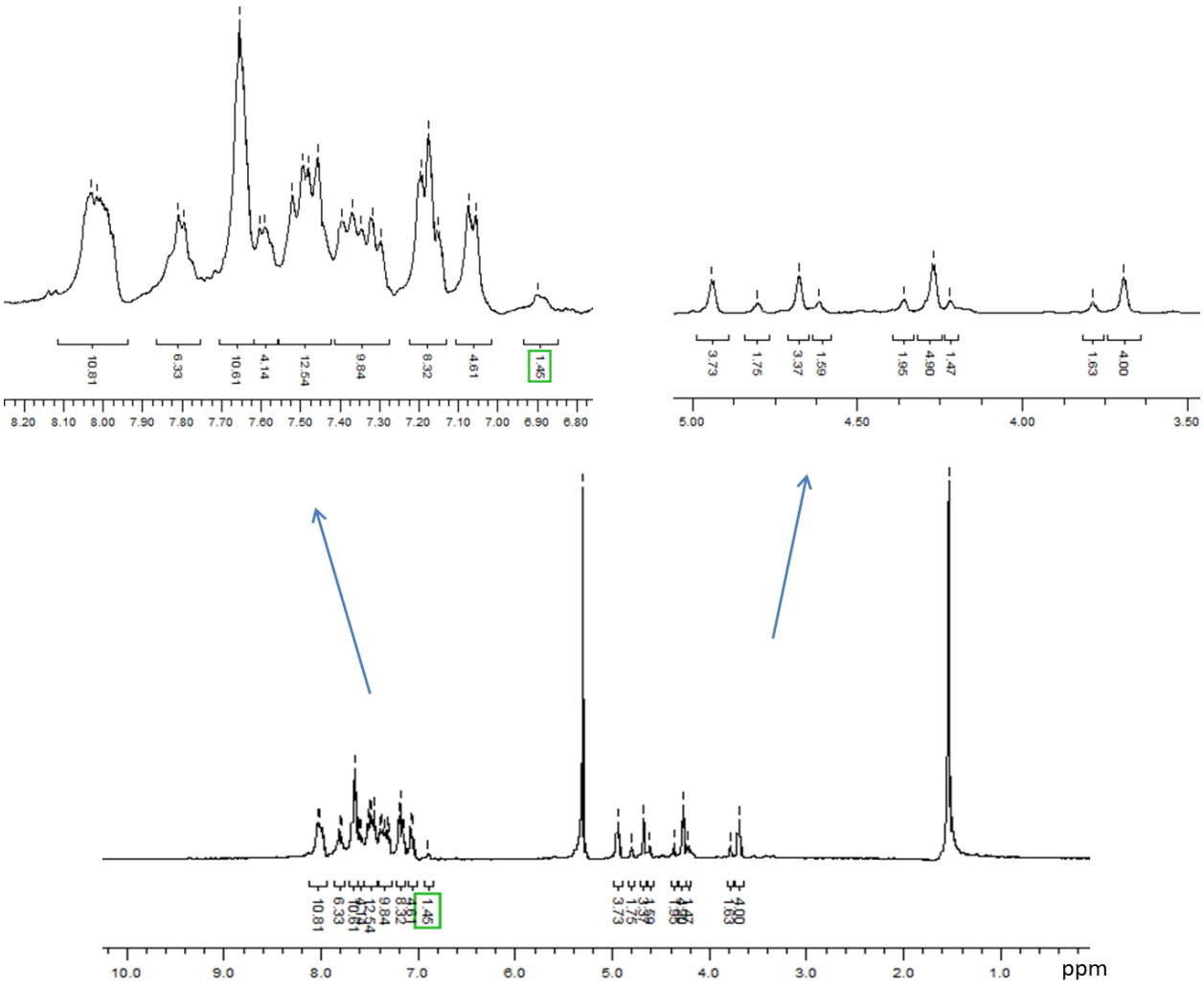

Fig. S15 ^{1}H NMR spectra (300 MHz, CD_2Cl_2) of $[Pt(dppf)(4\text{-}Sepy)]_n(OTf)_n$ (**9**).

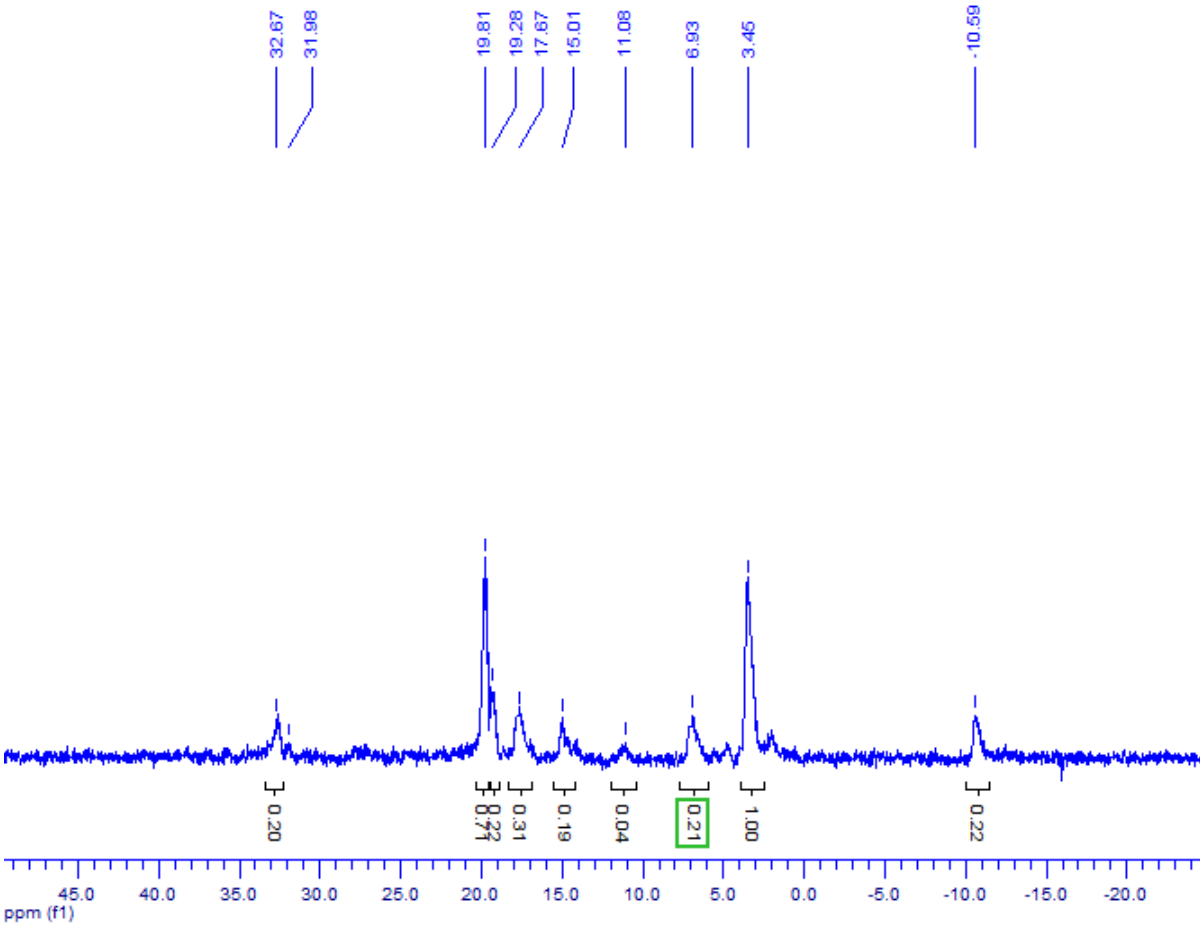

Fig. S16 $^{31}P\{^{1}H\}$ NMR spectra 121.5 MHz, CD_2Cl_2) of $[Pt(dppf)(4\text{-}Sepy)]_n(OTf)_n$ (**9**).

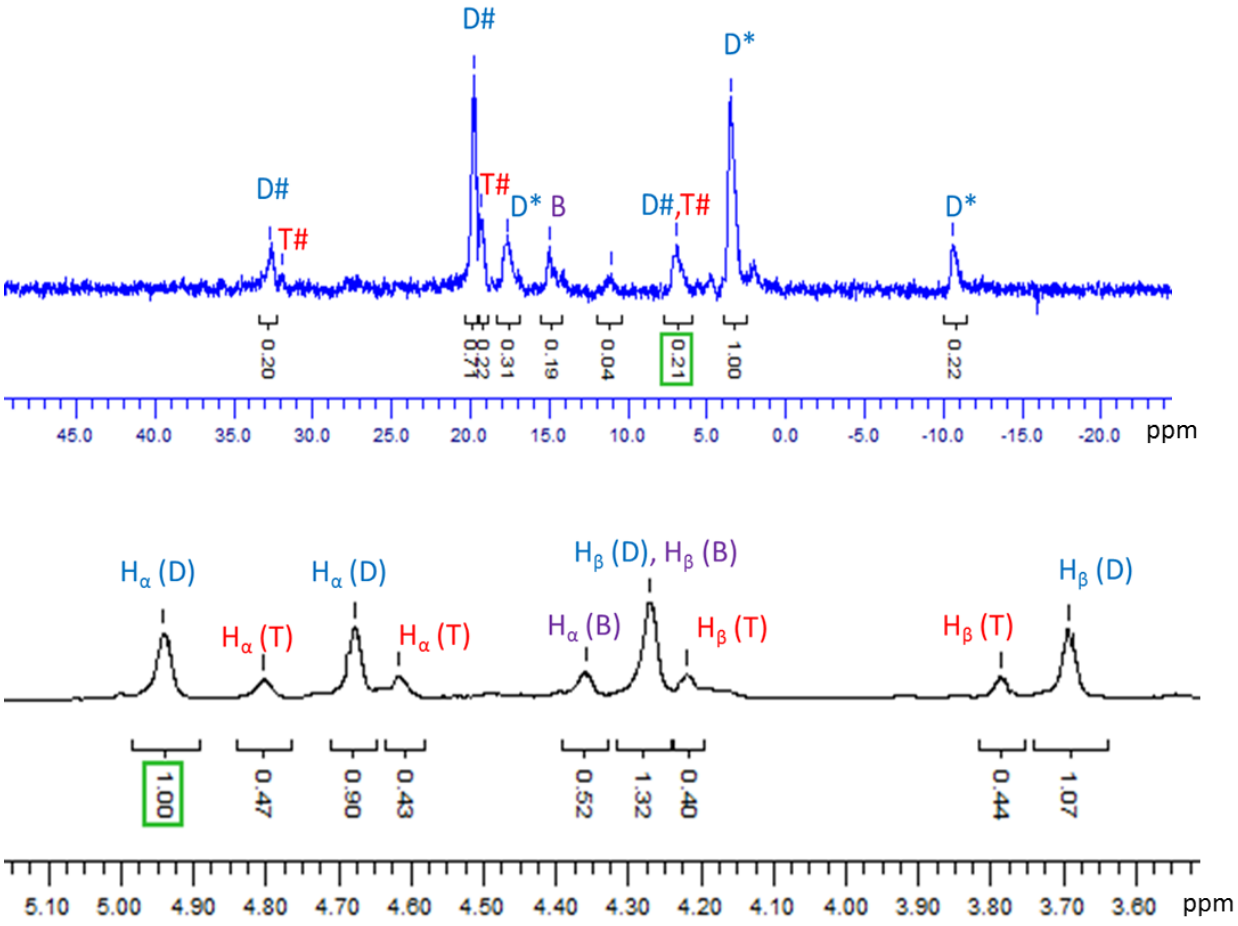

Fig. S17 (A) $^{31}P\{^{1}H\}$ NMR spectrum (121.5 MHz); (**B**) Ferrocenyl region of the ^{1}H NMR spectrum (300 MHz) of $[Pt(dppf)(4\text{-}SeC_5H_4N)]_n(OTf)_n$ (**9**) in CD_2Cl_2 (**D** = dimer **9D**, **T** = tetramer **9T**, **B** = bridging).

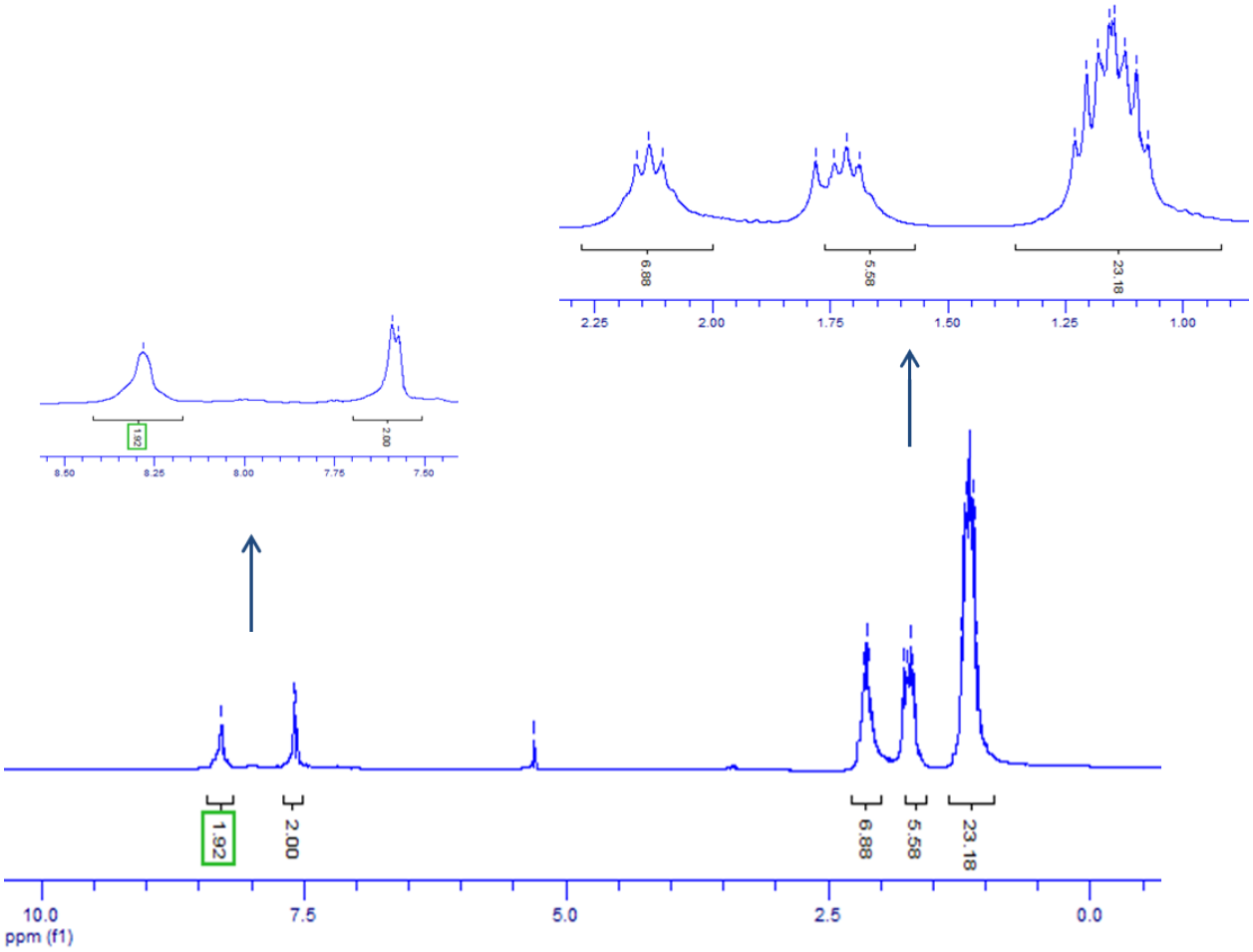

Fig. S18 ^{1}H NMR spectra (300 MHz, CD_2Cl_2) of $[Pt(PEt_3)_2(4\text{-Sepy})]_n(OTf)_n$ (**10**).

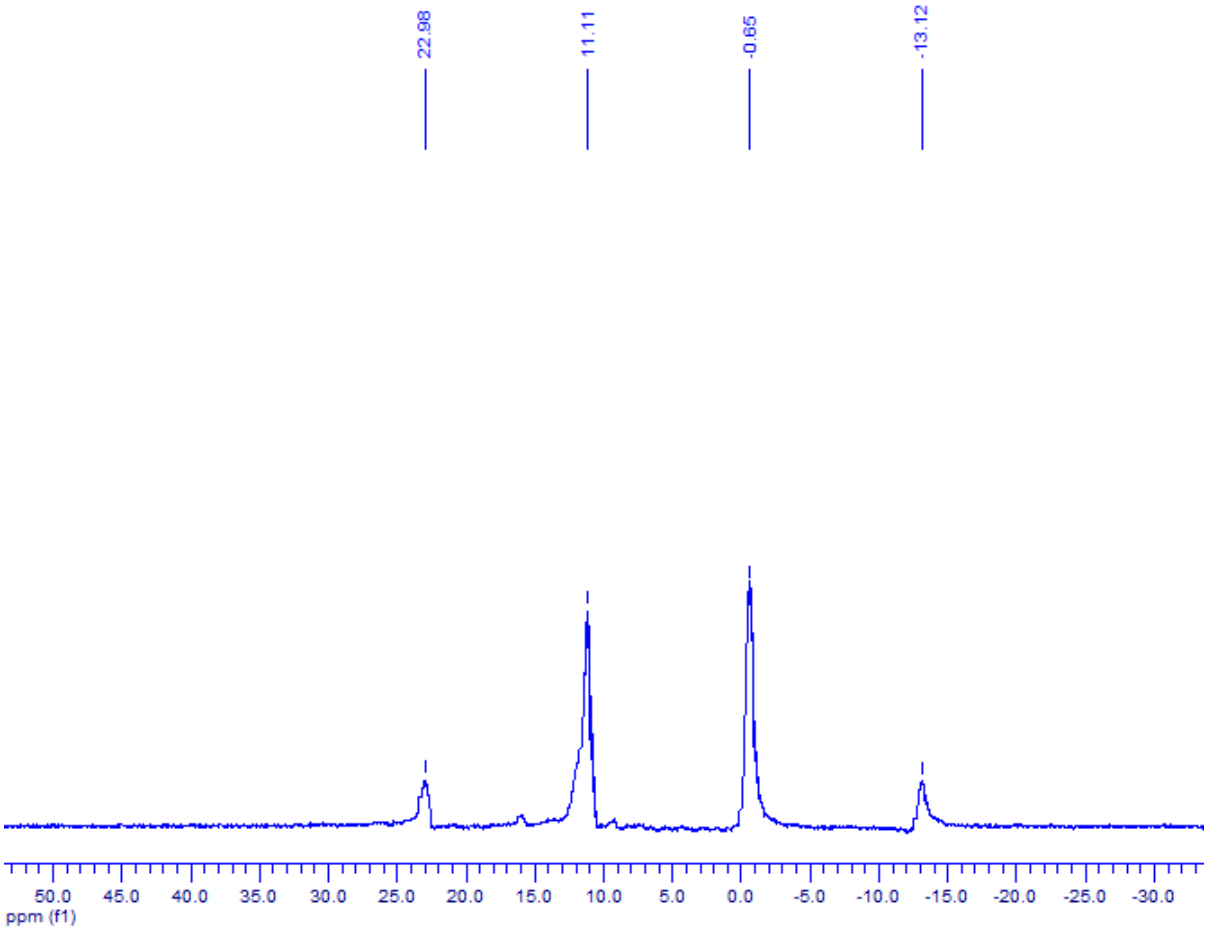

Fig. S19 $^{31}P\{^{1}H\}$ NMR spectra 121.5 MHz, CD_2Cl_2) of $[Pt(PEt_3)_2(4\text{-Sepy})]_n(OTf)_n$ (**10**).

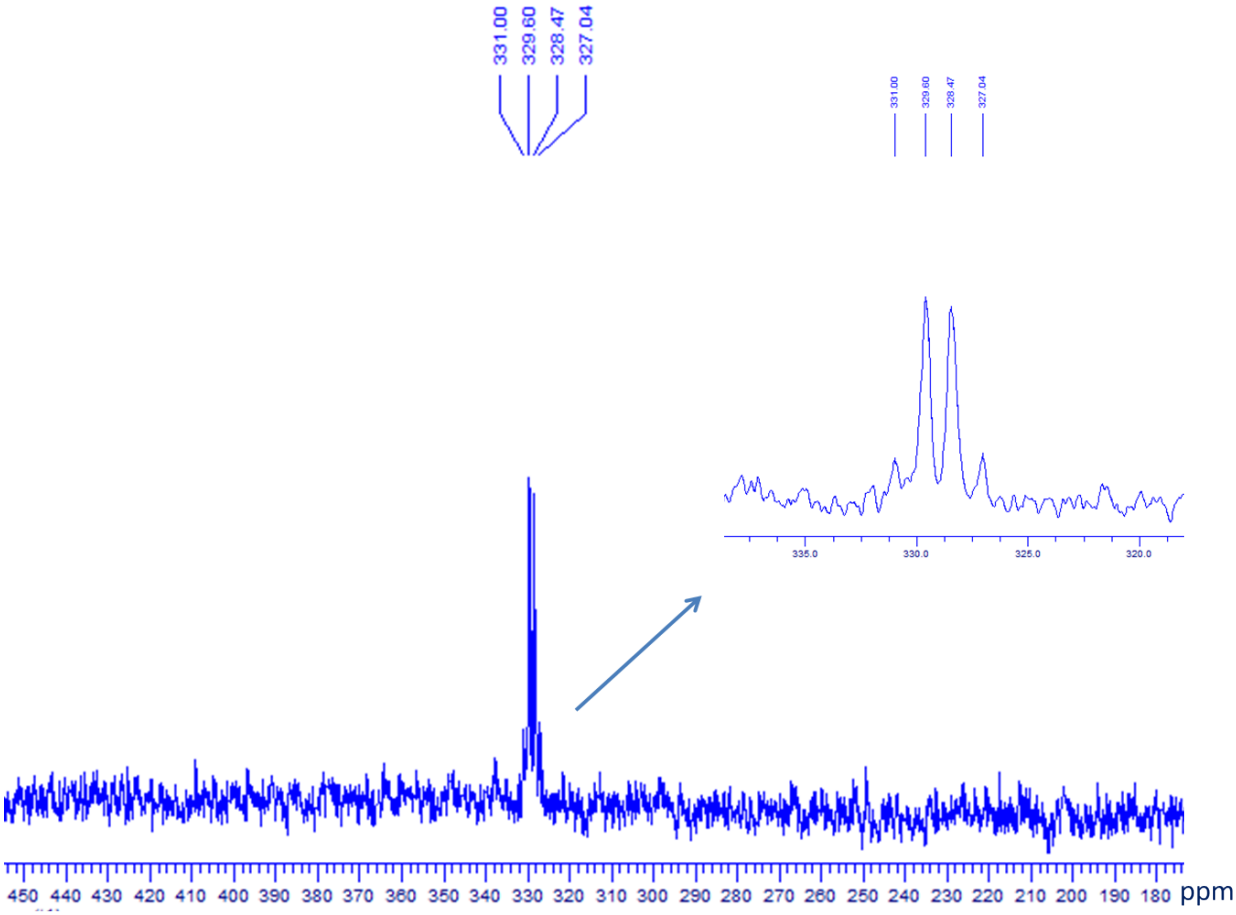

Fig. S20 $^{77}Se\{^{1}H\}$ NMR spectra 57.2 MHz, CD_2Cl_2) of $[Pt(PEt_3)_2(4\text{-Sepy})]_n(OTf)_n$ (**10**).

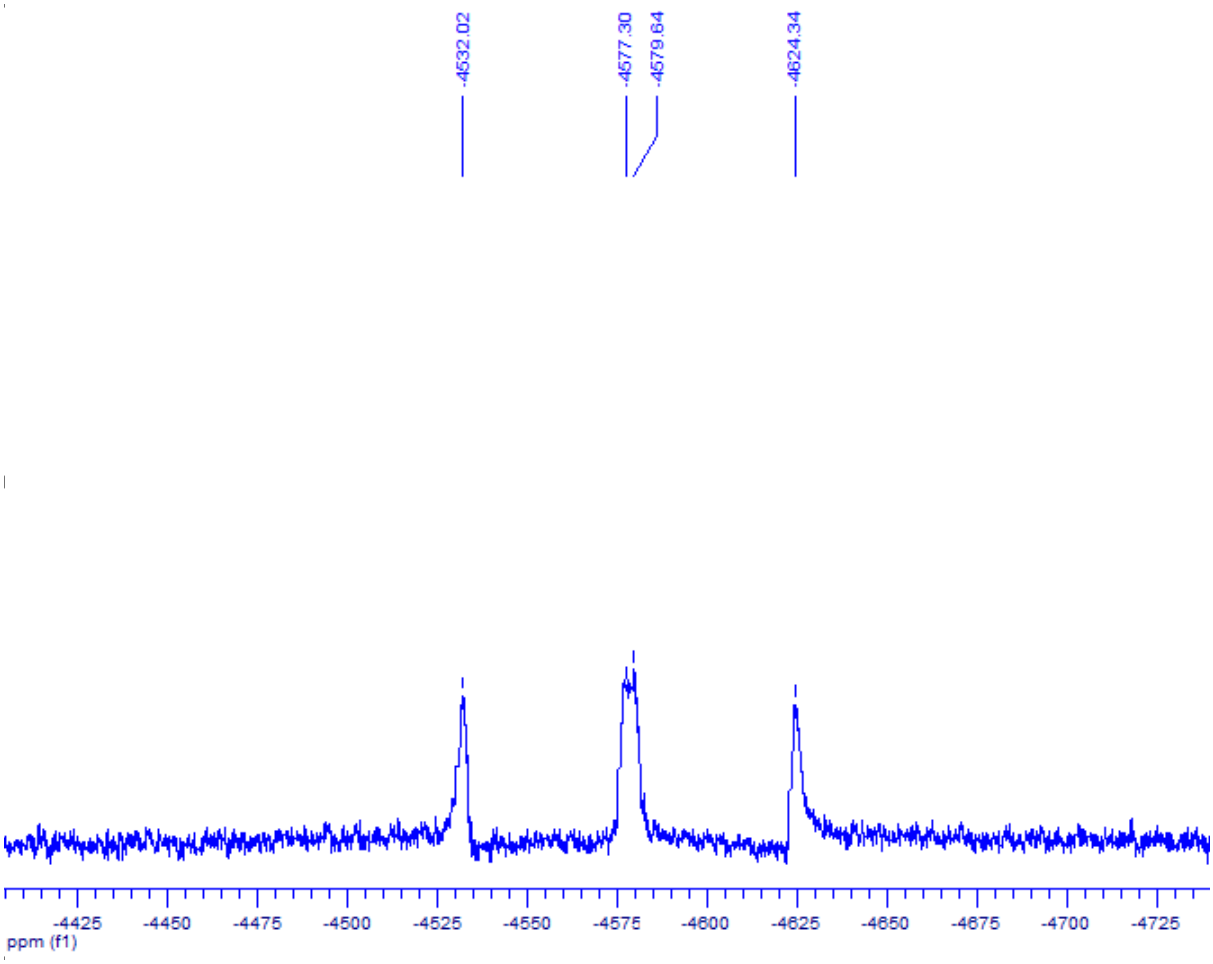

Fig. S21 $^{195}Pt\{^{1}H\}$ NMR spectra 64.5 MHz, CD_2Cl_2) of $[Pt(PEt_3)_2(4\text{-Sepy})]_n(OTf)_n$ (**10**).

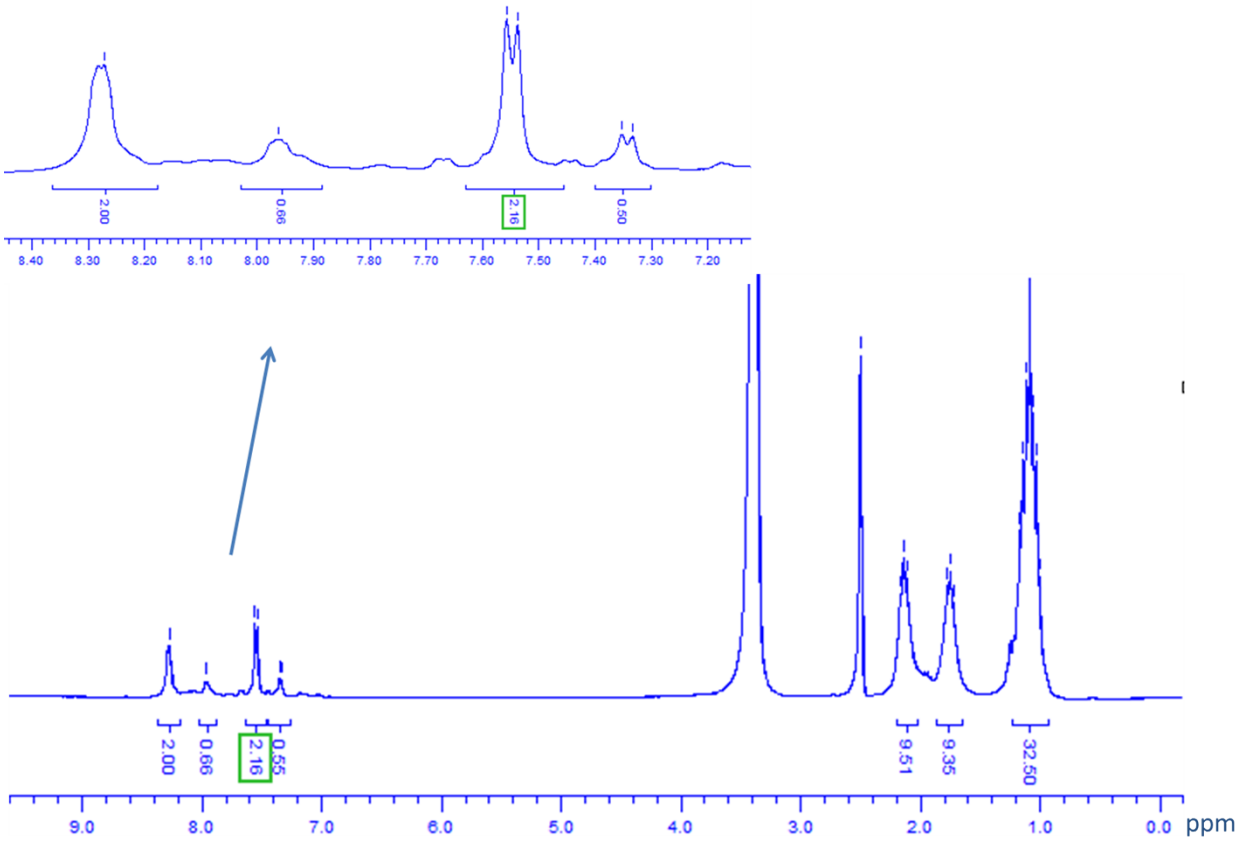

Fig. S22 ^{1}H NMR spectra (300 MHz, dmso-d_6) of $[Pt(PEt_3)_2(4\text{-Sepy})]_n(OTf)_n$ (**10**).

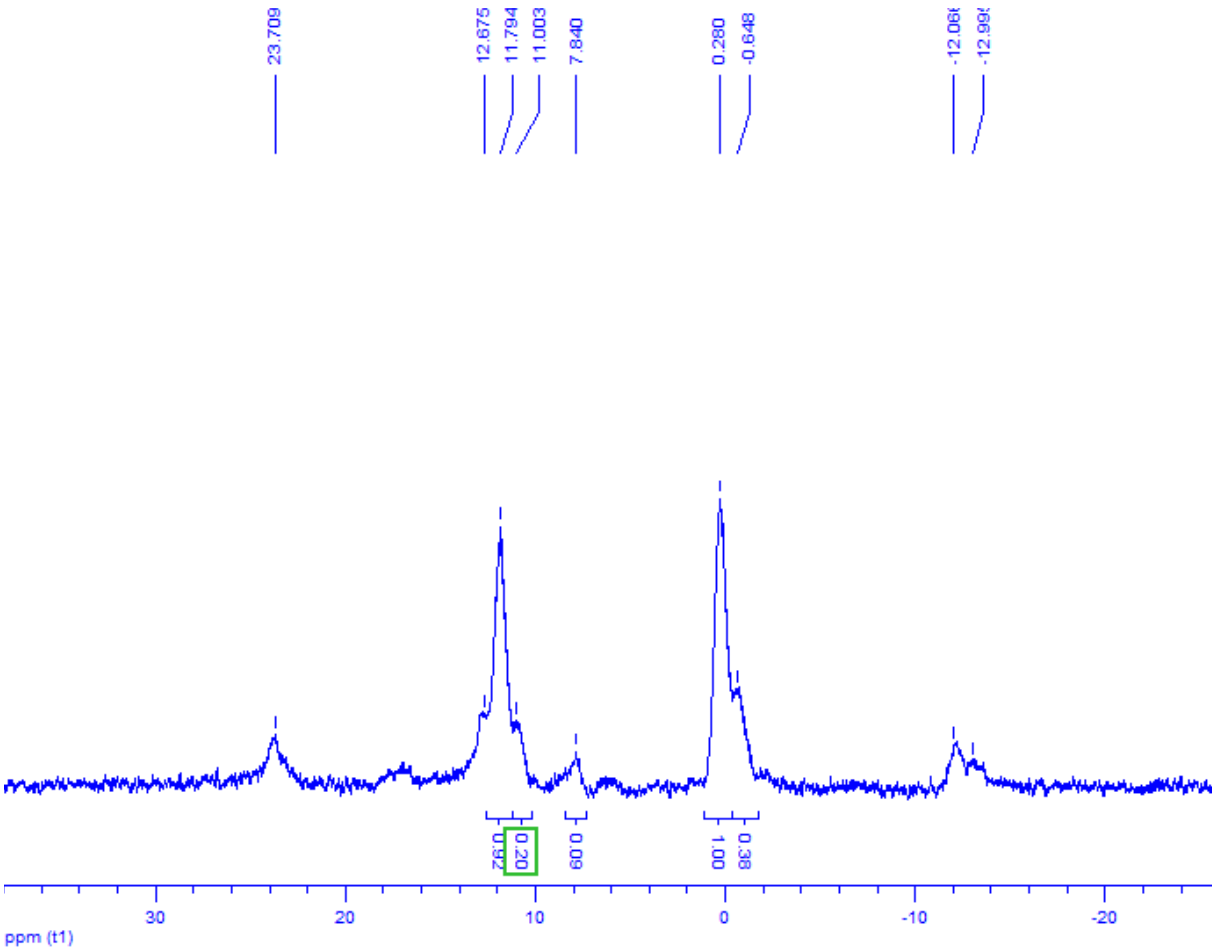

Fig. S23 $^{31}P\{^{1}H\}$ NMR spectra 121.5 MHz, dmso-d_6) of $[Pt(PEt_3)_2(4\text{-Sepy})]_n(OTf)_n$ (**10**).

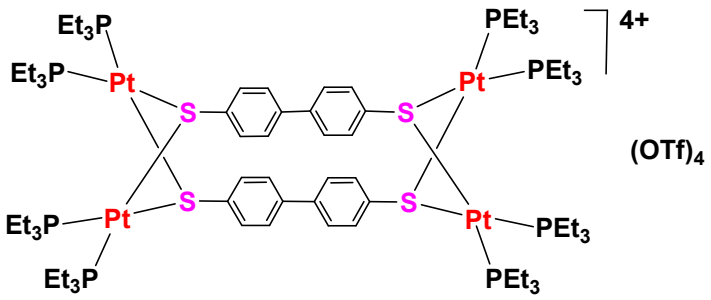

Scheme S1 Structural drawing of $[Pt_2(PEt_3)_4(S(C_{12}H_8)S)]_2(OTf)_4$ (**11**)

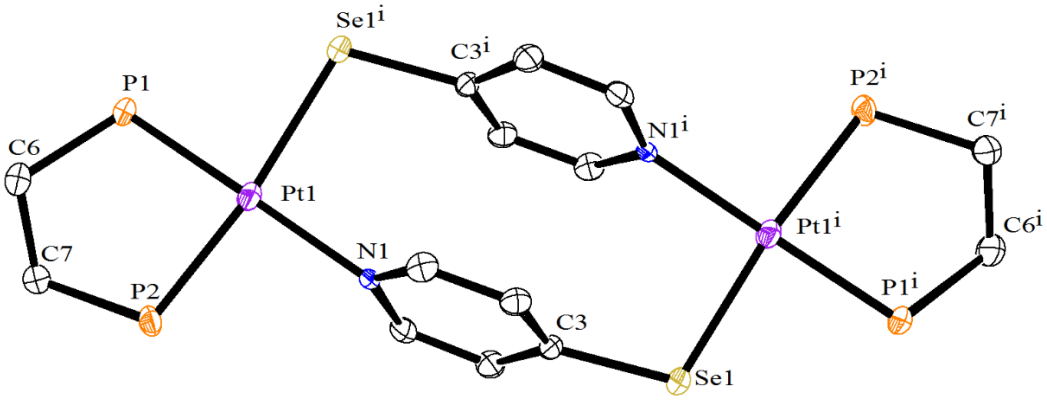

Fig. S24 ORTEP diagram of $[Pt(dppe)(4\text{-}Sepy)]_2(BPh_4)_2$ (**12D**) ellipsoids drawn at 50% probability. The hydrogen atoms, dppe phenyl groups, and BPh_4 ions are omitted for clarity.

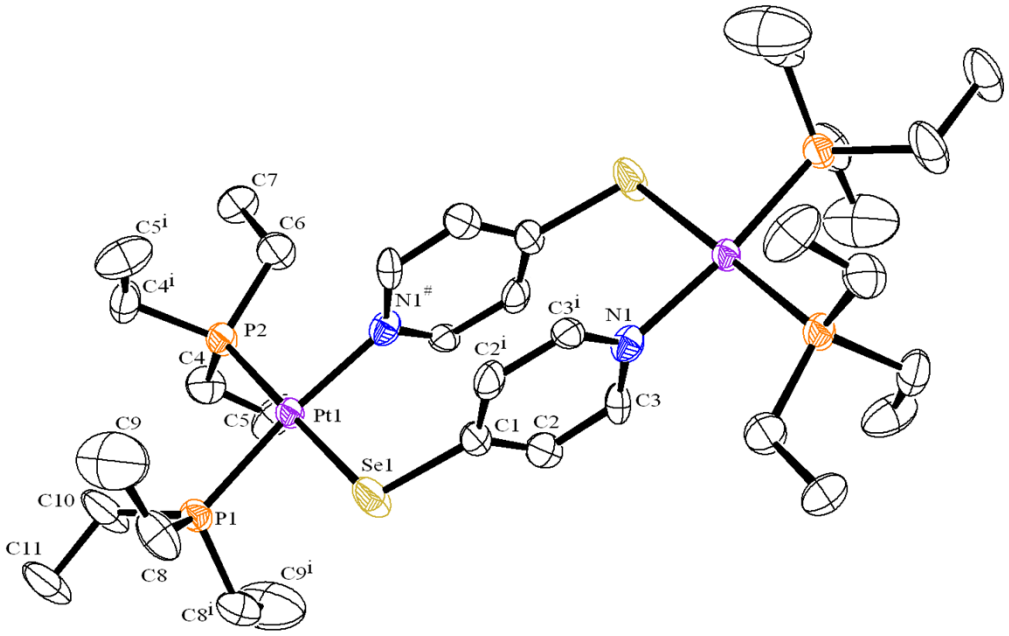

Fig. S25 ORTEP diagram of $[Pt(PEt_3)_2(4\text{-Sepy})]_2(BPh_4)_2$ (**13D**) ellipsoids drawn at 50% probability. The BPh_4 ions were masked. The hydrogen atoms are omitted for clarity.

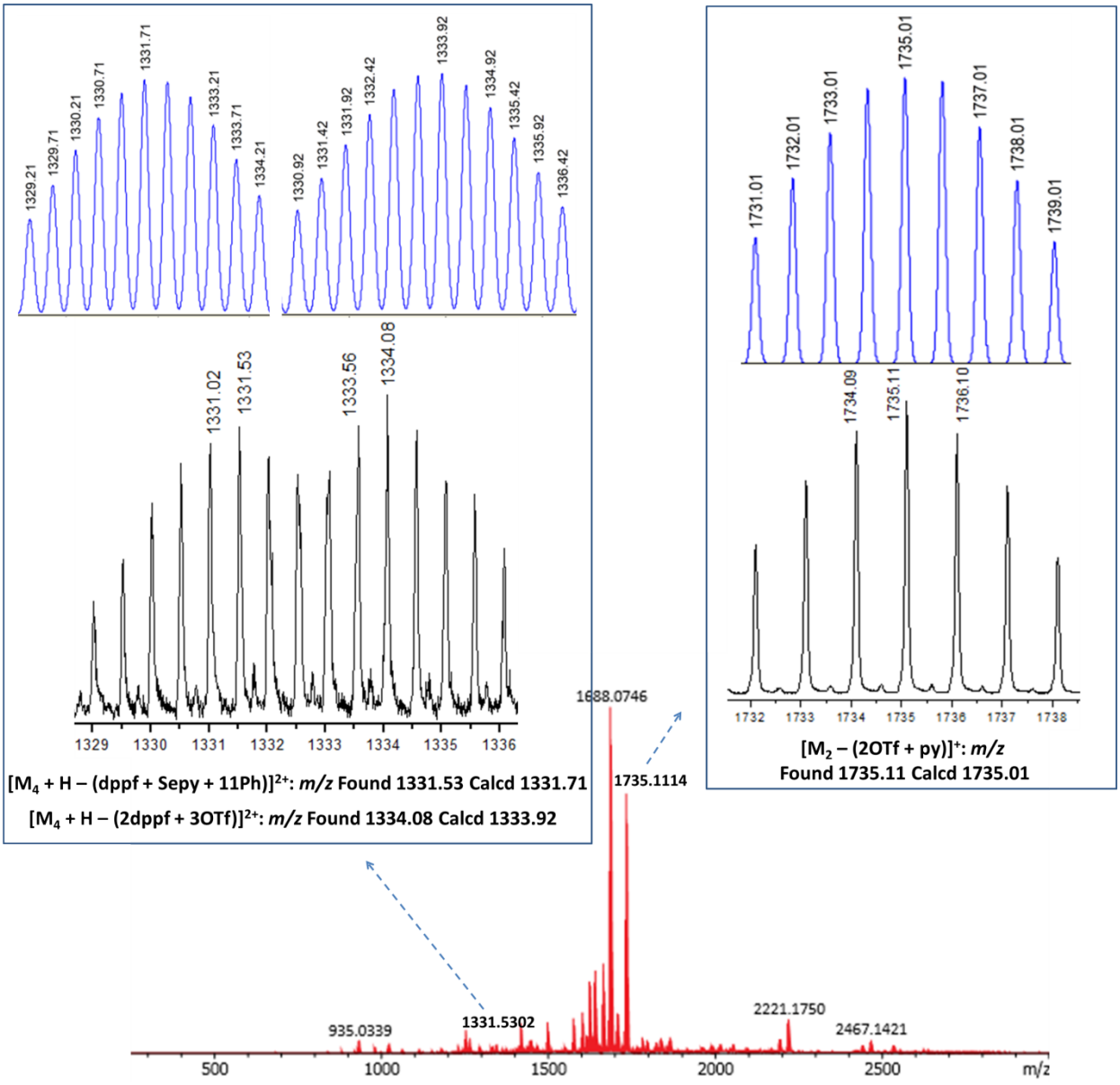

Fig. S26 ESI-mass spectrum of $[Pt(dppf)(4\text{-}Sepy)]_n(OTf)_n$ (**9**). The insets show the experimentally obtained (below) isotope patterns of the fragments with those simulated (above) on the basis of natural isotope abundances. The found and calcd values are for the most abundant peak of ion.

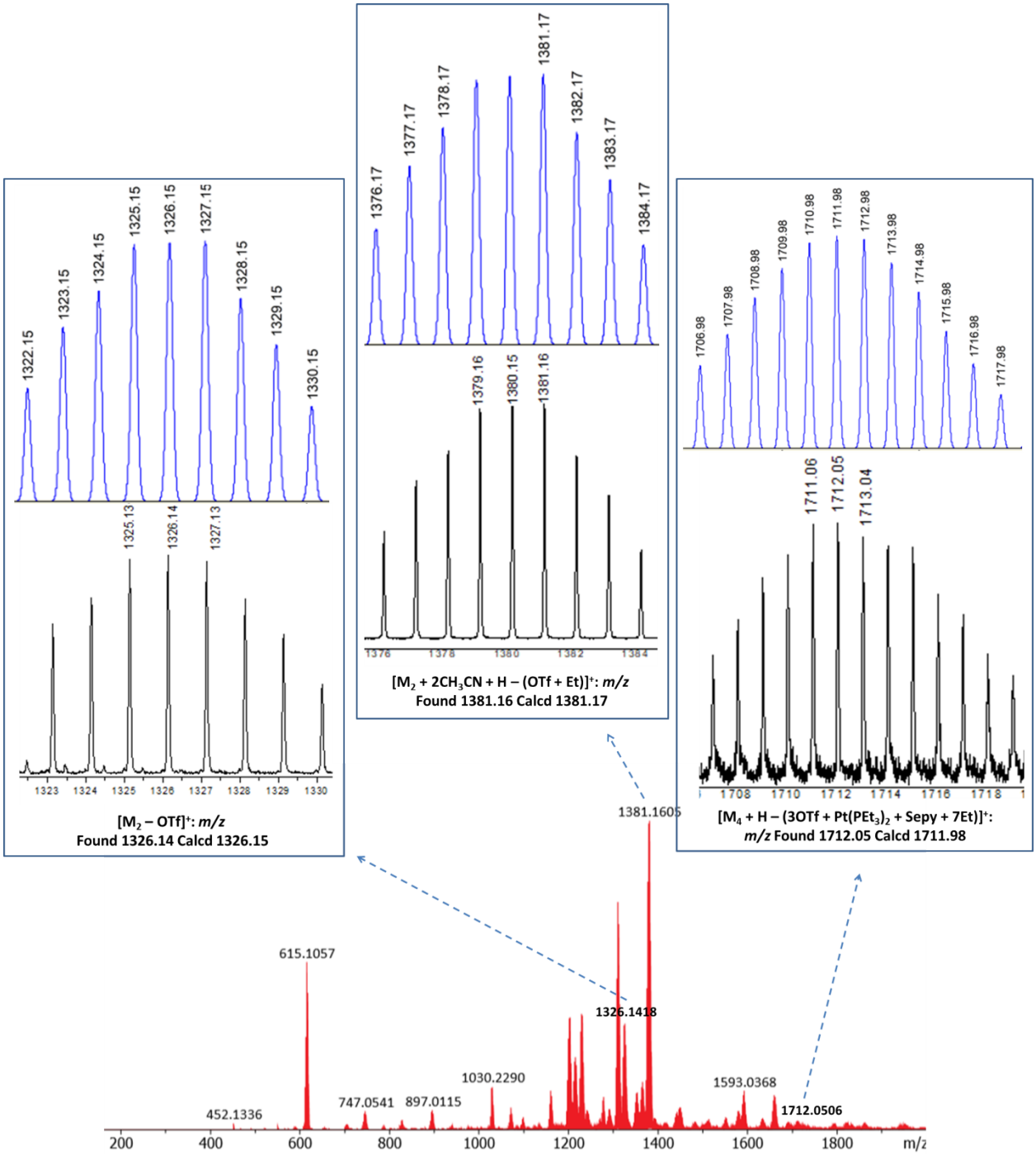

Fig. S27 ESI-mass spectrum of $[Pt(PEt_3)_2(4\text{-Sepy})]_n(OTf)_n$ (**10**). The insets show the experimentally obtained (below) isotope patterns of the fragments with those simulated (above) on the basis of natural isotope abundances. The found and calcd values are for the most abundant peak of ion.

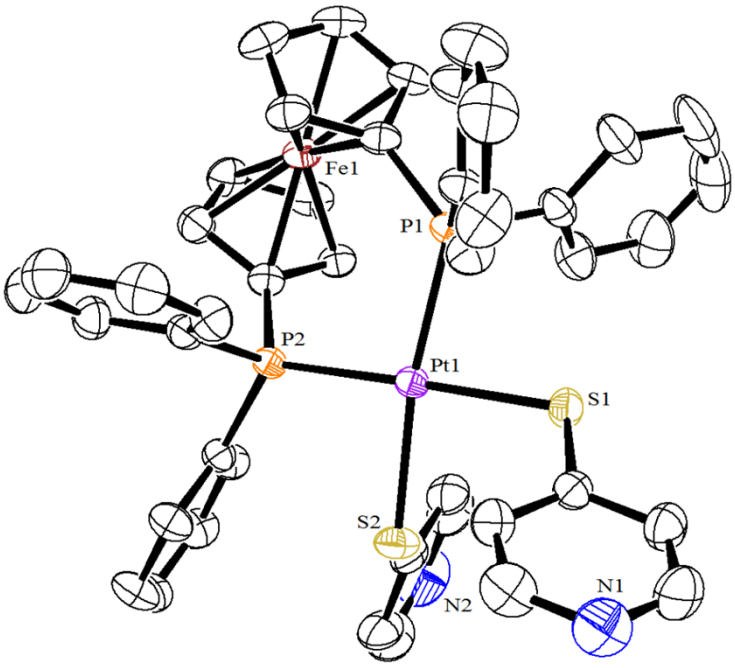

Fig. S28 ORTEP diagram of [Pt(dppf)(4-Spy)$_2$] (**1**) ellipsoids drawn at 35% probability. The hydrogen atoms are omitted for clarity.

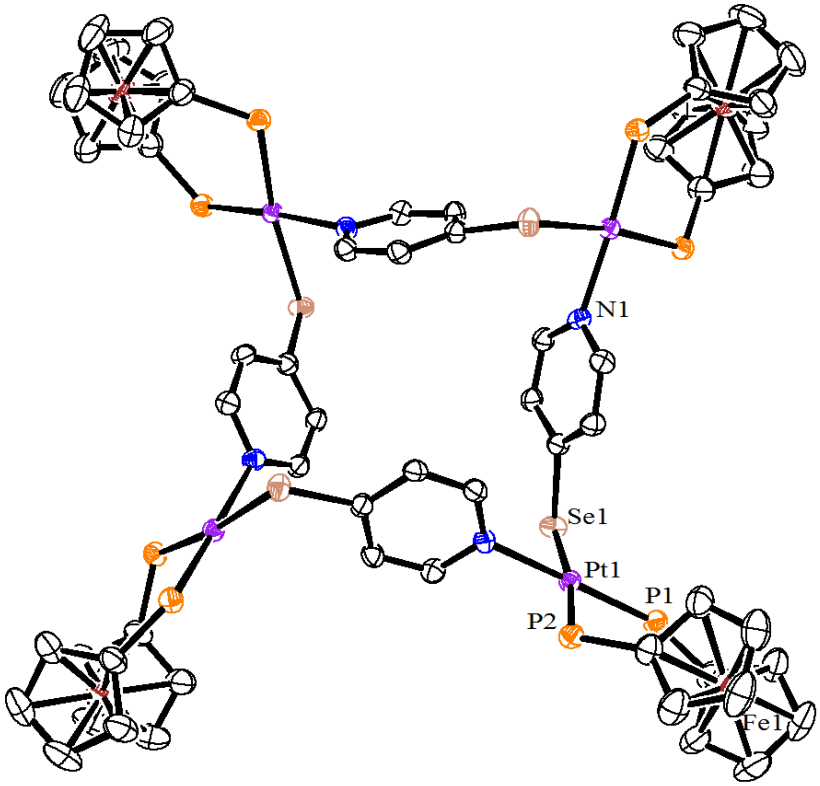

Fig. 29 ORTEP diagram of $[Pt(dppf)(4\text{-}Sepy)]_4(OTf)_4$ (**9T**) ellipsoids drawn at 35% probability. The dppf phenyl groups, hydrogen atoms, and triflate ions are omitted for clarity.

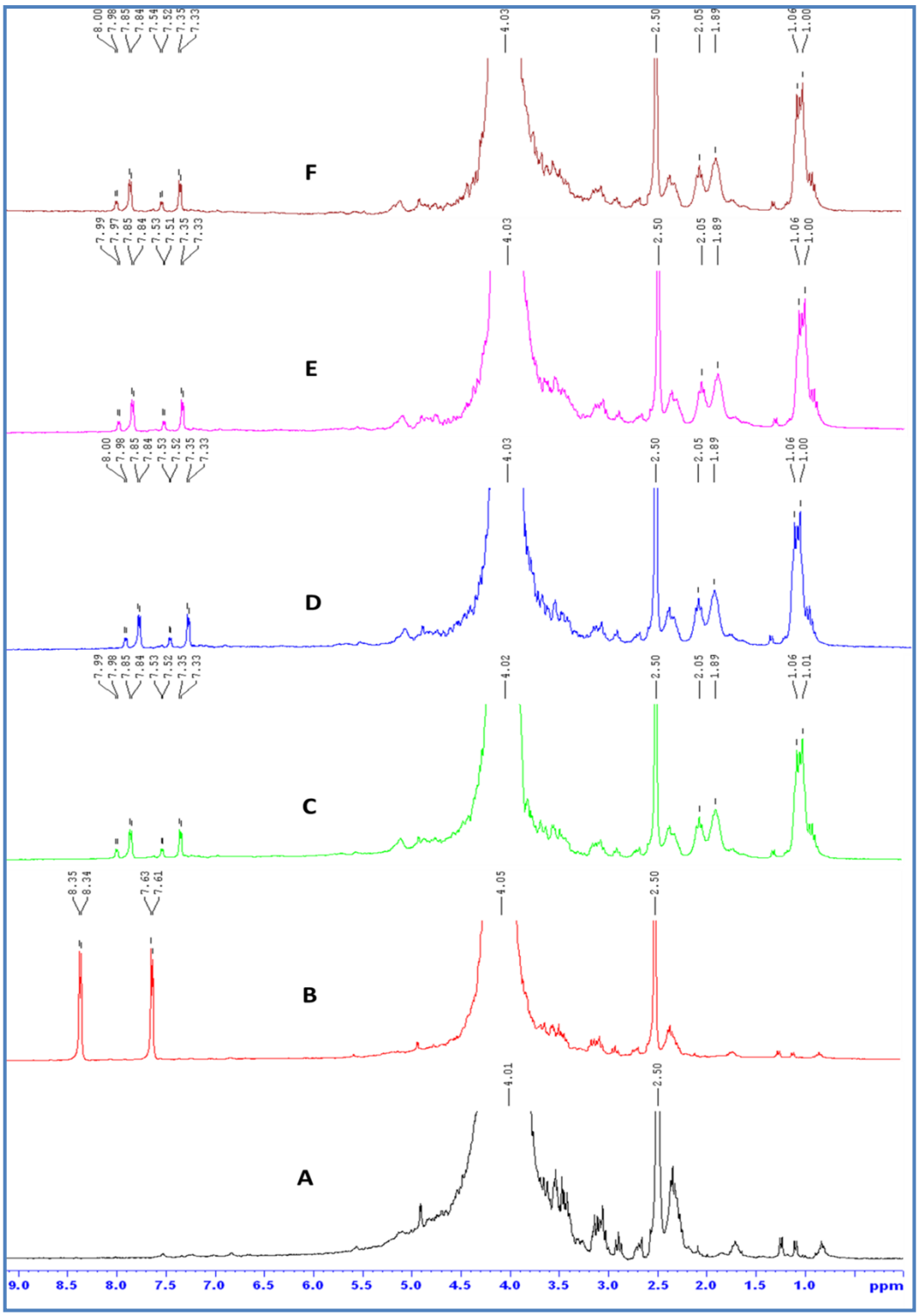

Fig. S30 ^{1}H NMR spectra (300 MHz) of A) mixture of cell culture medium and DMSO-d_6 (1:4, v/v), B) with 4,4′-py_2Se_2 (free ligand), and with the $[Pt(PEt_3)_2(4\text{-}Sepy)]_n(OTf)_n$ (**10**), C) immediately, after D) 6 h, E) 1 day and F) 3 days in the mixture of culture medium and DMSO-d_6 (1:4, v/v).

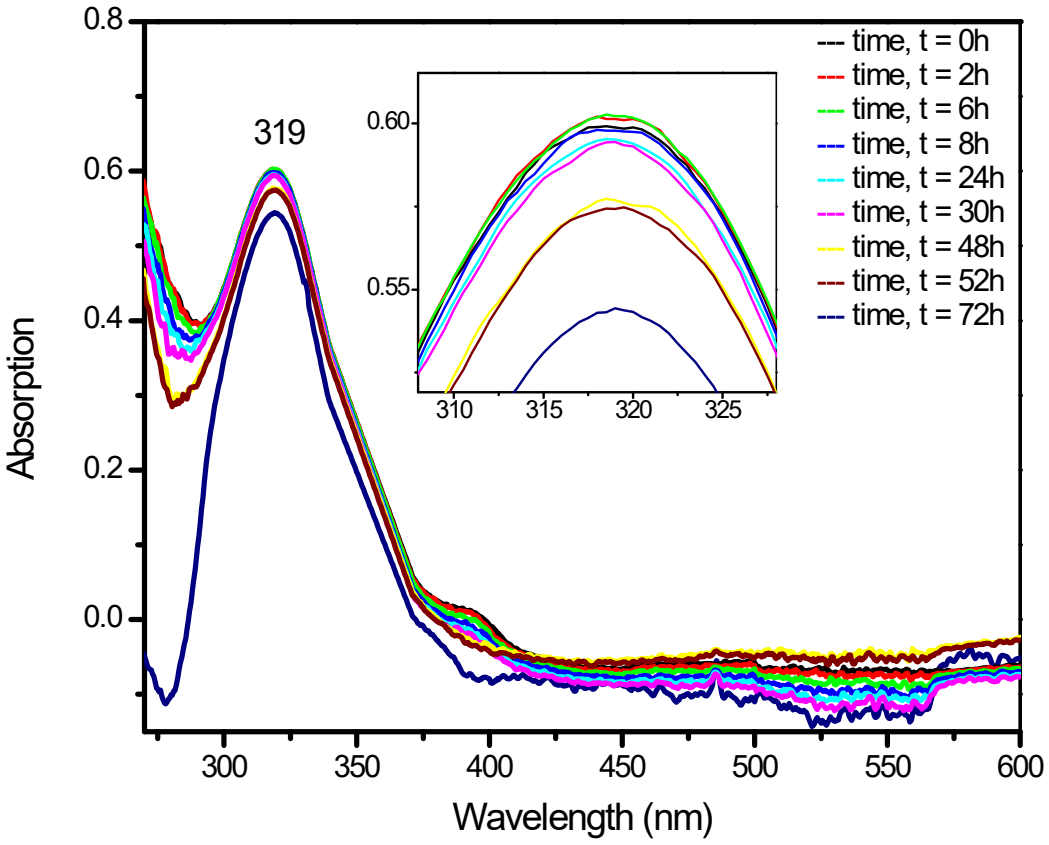

Fig. S31 UV-Vis spectra of $[Pt(PEt_3)_2(4\text{-Sepy})]_n(OTf)_n$ (**10**) in mixture of cell culture medium and DMSO (1:4, v/v) overtime scale.

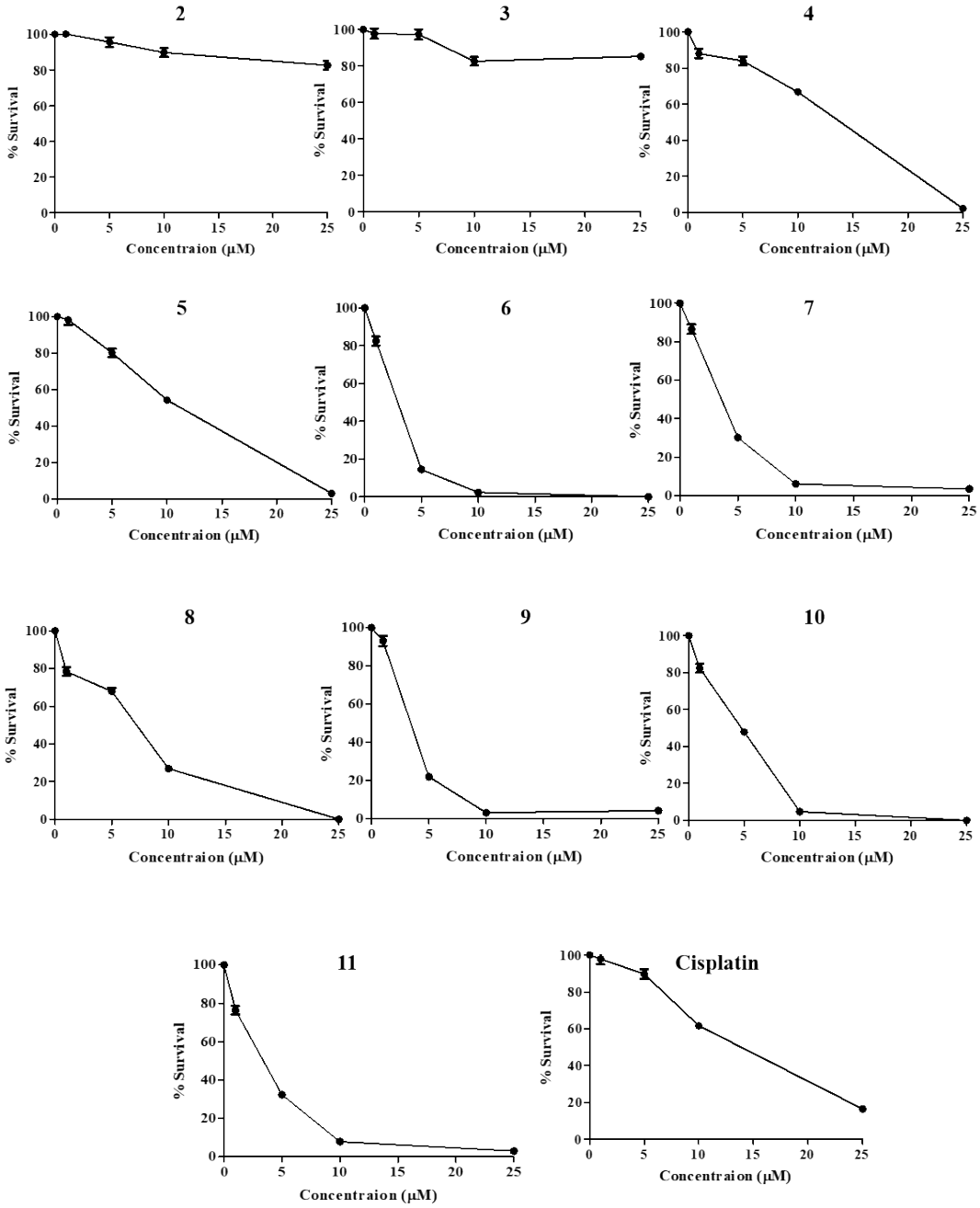

Fig. S32 Dose response curves of the different synthesized compounds against MCF7 cells determined by MTT assay. Cells were treated with 1, 5, 10 or 25 µM of each compound for 48 hours, followed by determination of cellular viability by MTT assay.

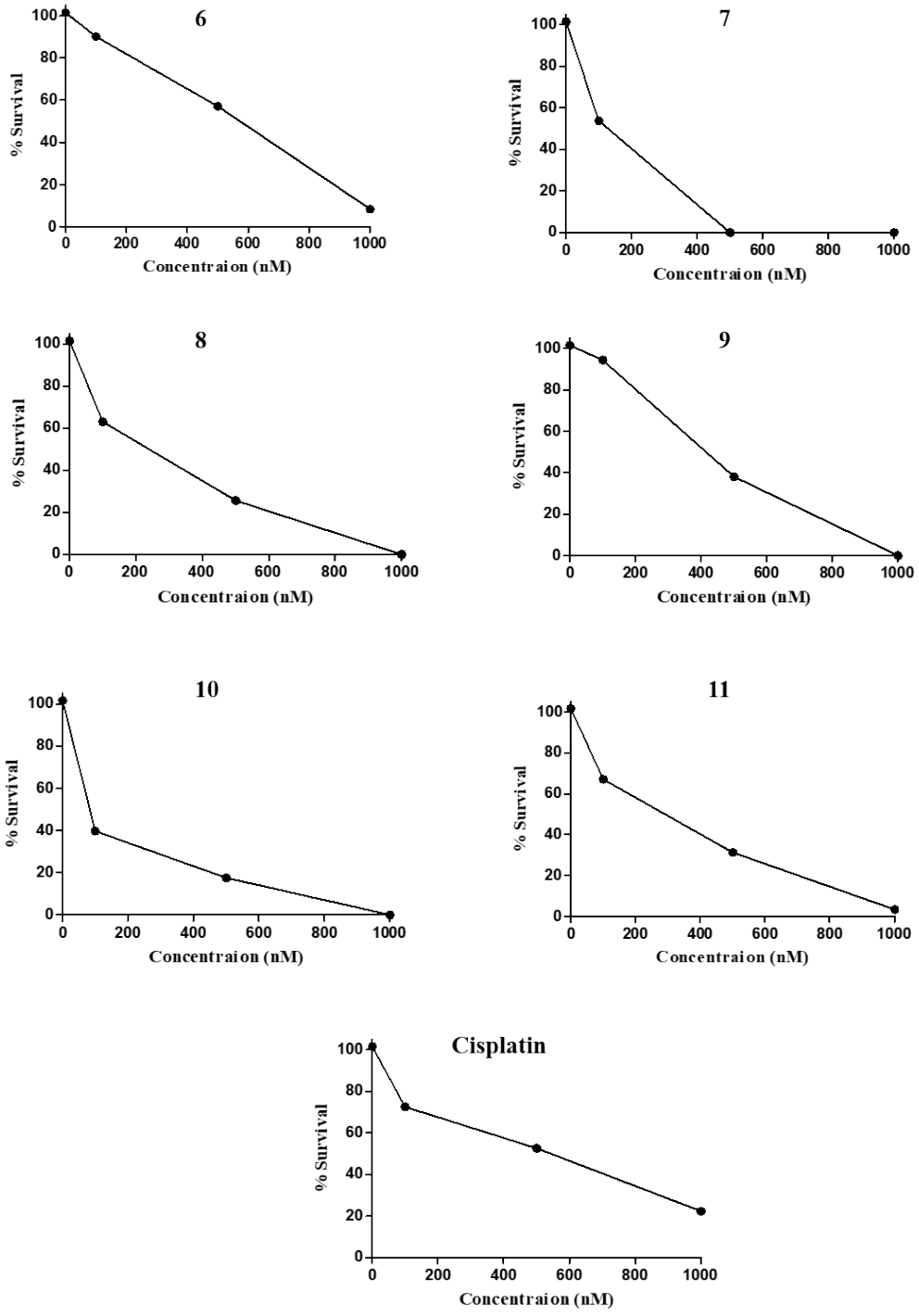

Fig. S33 Dose response curves of shortlisted compounds against MCF7 cells determined by clonogenic assay. Cells were incubated with 100, 500 or 1000 nM of each compound for 14 days, followed by staining of colonies with crystal violet and quantification of the number of colonies containing >30 cells under a light microscope.

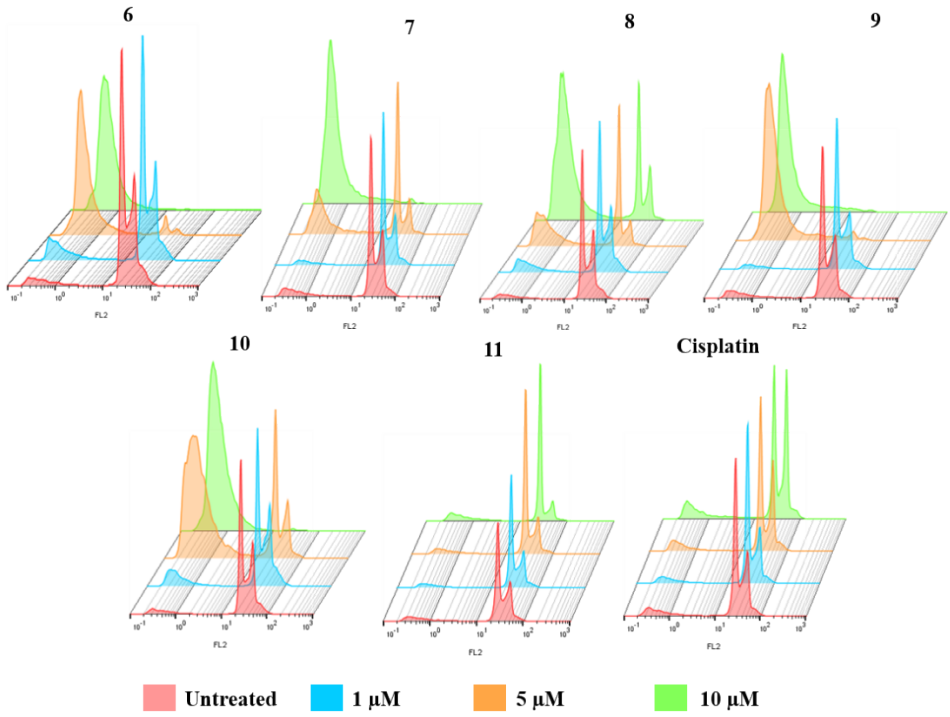

Fig. S34 Histograms representing Sub G1 analysis of MCF7 cells treated with the different compounds. Cells were treated with indicated concentrations of each compound for 48 hours, followed by Sub G1 analysis employing flow cytometry.

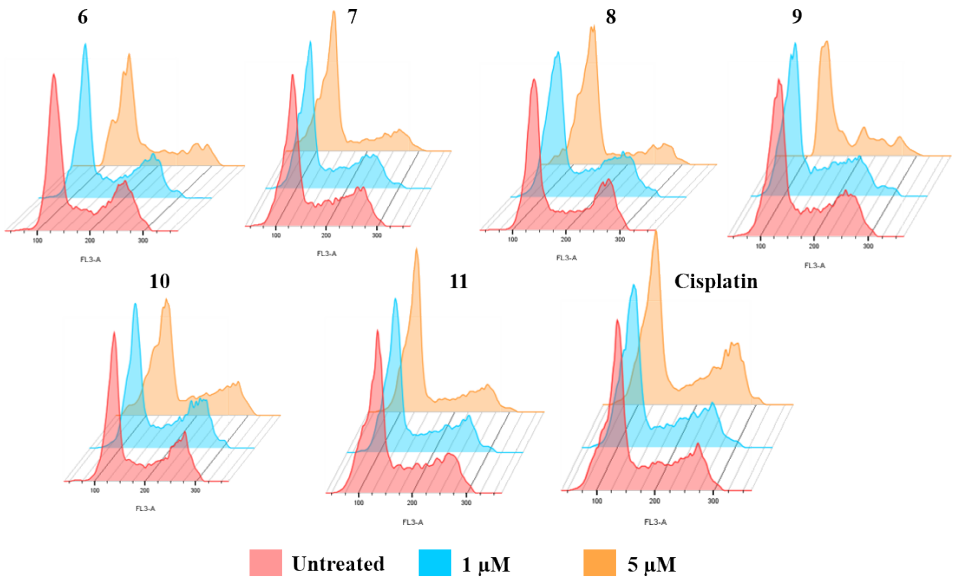

Fig. S35 Cell cycle analysis of MCF7 cells treated with indicated concentrations of the different compounds. Cells were treated with 1 or 5 µM of each compound for 24 hours, followed by analysis of cell cycle distribution using flow cytometry.